Optimization of Cas12a for multiplexed genome-scale transcriptional activation

Audrey L Griffith[1,2], Fengyi Zheng[1,2], Abby V McGee[1,2], Nathan Miller[1], Zsofia M Szegletes[1], Ganna Reint[1], Fabian Gademann[1], Ifunanya Nwolah[1], Mudra Hegde[1], Yanjing V Liu[1], Amy Goodale[1], John G Doench[1]*

[1] Genetic Perturbation Platform, Broad Institute of MIT and Harvard, 75 Ames St., Cambridge, MA
[2] These authors contributed equally
* Correspondence to jdoench@broadinstitute.org

ABSTRACT

Cas12a CRISPR technology, unlike Cas9, allows for facile multiplexing of guide RNAs from a single transcript, simplifying combinatorial perturbations. While Cas12a has been implemented for multiplexed knockout genetic screens, it has yet to be optimized for CRISPR activation (CRISPRa) screens in human cells. Here we develop a new Cas12a-based transactivation domain (TAD) recruitment system using the ALFA nanobody and demonstrate simultaneous activation of up to four genes. We screen a genome-wide library to identify modulators of growth and MEK inhibition and we compare these results to those obtained with open reading frame (ORF) overexpression and Cas9-based CRISPRa. We find that the activity of multiplexed arrays is largely predictable from the best-performing guide and provide criteria for selecting active guides. We anticipate that these results will greatly accelerate the exploration of gene function and combinatorial phenotypes at scale.

INTRODUCTION

CRISPR technology was rapidly engineered to enable a range of genomic manipulations beyond gene knockout (CRISPRko), including at the level of transcription with gene activation (CRISPRa) and interference (CRISPRi)[1,2]. Building off prior studies with zinc fingers and TALEs[3–5], Cas9-based CRISPRa approaches have employed transactivation domains (TADs) such as VP64 or P300 directly fused to deactivated Cas9 (dCas9)[6,7]. Additionally, the SAM and Suntag systems recruit TADs in trans via motifs appended to the tracrRNA and dCas9, respectively[8,9]. Heterologous combinations of TADs have also been developed, such as VPR, which combines VP64, p65, and Rta[10] domains, and recent studies have explored the landscape of potential TADs in high throughput[11–13].

CRISPRa technology has been deployed for genome-wide genetic screens across a diversity of phenotypes. Comparison to matched CRISPRko and CRISPRi screens shows that CRISPRa does not simply provide the mirror image of depletion approaches but rather implicates many new genes, providing a fuller understanding of cellular circuitry[14,15]. CRISPRa has its challenges, however, as certain TADs can lead to toxicity, as well as vary in their efficacy across different gene targets and cell lines[16], perhaps because endogenous promoters have differing cofactor requirements[17]. Further, heterogeneity of transcription start site (TSS) usage

and ambiguity in annotation across cell types[18], especially in less well-characterized model systems, can lead to a large number of ineffective reagents, decreasing the power and effective coverage of guide libraries.

Previously, we reported the optimization of an enhanced version of Cas12a from *Acidaminococcus sp*. (enAsCas12a, herein referred to simply as Cas12a) for some-by-some combinatorial screens and genome-wide single gene screens[19,20]. This approach compares favorably to Cas9-based screens largely because several guides can be easily multiplexed in a single vector, resulting in a more compact library while still benefiting from numerous 'shots on goal' for each gene. Further, the production of erroneous hybrid vectors due to lentiviral swapping is a significant concern for dual-Cas9 vectors, where such confounders can represent up to 29% of a pooled library[21–23]. As the rate of swapping is distance-dependent, this concern is minimized with the Cas12a architecture as individual guides are separated by only a 20 nucleotide direct repeat (DR), compared to several hundred nucleotides with Cas9 guide cassettes. We and others have leveraged these advantages of Cas12a to explore synthetic lethality[19,24] and paralog redundancy[25,26] by targeting multiple genes simultaneously.

Prior work with Cas12a for CRISPR activation has shown that direct tethering of various TADs, including VPR, VP64, p65, and 'Activ' (a set of three modified p65 domains along with HSF1) to deactivated Cas12a (dCas12a) leads to varying levels of transcriptional activation[27]. But as yet there has been no demonstration of highly penetrant activity when delivering the components by lentivirus – that is, activation of a gene target in a large fraction of cells that receive the machinery – which is a prerequisite for effective genetic screens. Thus, we set out to develop Cas12a as a suitable approach for CRISPRa screens.

RESULTS

Evaluation of existing Cas12a CRISPRa technologies

To measure the activation efficiency of CRISPRa with Cas12a we first required a guide targeting a gene whose expression could be readily assessed. We opted for a cell surface marker, as magnitude of effect across a population of cells could be measured via flow cytometry; unlike qRT-PCR, flow cytometry can distinguish between a small number of cells with substantial upregulation of a target gene or a large number of cells with a weaker response. We thus designed a small pooled library containing 10 guides targeting the cell surface marker CD4, which is poorly expressed in most cell lines, and 20 control guides targeting olfactory receptors. All guides were paired with one another in a single cassette to generate a dual-guide library. To identify candidate CD4 guides with strong activity, we screened this library in HCC2429 cells stably expressing Cas12a with a deactivating D908A mutation tethered to a modified version of the VPR TAD containing VP64, p65, and a shortened Rta domain[28]. We observed a small fraction of cells expressing CD4 (1.8%) on day ten following transduction, and a general toxicity associated with the expression of VPR, which others have reported[16]. Nevertheless, we performed flow cytometry and collected the CD4-expressing cell population and the middle 10% of the non-CD4 expressing population from which we isolated genomic DNA, retrieved the guides using PCR, and sequenced to determine the abundance of guides in

each population. Of the ten CD4-targeting guides in the library, one was clearly enriched in the positive population (Supplementary Figure 1a). We chose this guide, along with the second most enriched guide, and paired them on a single expression cassette for future experiments.

Two different point mutations have been employed to deactivate the DNase activity of Cas12a, D908A and E993A, and we sought to compare their activity for CRISPRa purposes. We tested 12 CRISPRa implementations with each nuclease-inactive variant by appending different TADs at the N' and C' termini, with violet-excited GFP (VexGFP) as a transduction marker. To ensure against over-optimization to one cell type, we employed HT29 cells for this experiment. Five days after delivery of the guides, we assessed CD4 expression levels via flow cytometry; a representative example of the gating strategy is provided (Supplementary Figure 1b). We observed that the D908A mutant consistently led to a higher fraction of CD4-positive cells (Figure 1a) and thus we employed this version (hereafter simply dCas12a) in all following experiments.

We next attempted to identify the optimal combination of directly tethered TADs, configurations of these TADs, and the location of nuclear localization sequences (NLSs). Using both the percentage of CD4-positive cells and the mean fluorescence intensity (MFI) of CD4 normalized to basal expression in HT29 cells, we compared activity of these 12 vectors. We observed no substantial differences in CD4 activation between constructs with the same TADs when the NLS was located either before or after the TAD on the C-terminus, indicating that the position of the NLS on the C' terminus is not of great importance when tethered to dCas12a. We observed that the Activ domain led to lower levels of CD4 activation than the VP64 domain in every case. Additionally, tethering two VP64 domains to dCas12a moderately improved CRISPRa activity compared to a single VP64 (Figure 1b).

We selected the top two combinations of domains – one VP64 domain on the C-terminus only or one VP64 domain on each terminus – for use in screens to identify additional effective guides. We also replaced the VexGFP marker with blasticidin resistance. We designed a library with numerous guides targeting the promoter regions of 13 genes coding for cell surface proteins (not all of which were assessed here). We tranduced this library into both HT29 and A375 cells expressing dCas12a-VP64 or VP64-dCas12a-VP64, each in a single biological treatment, treating the two dCas12a constructs as quasi-replicates (Figure 1c). On day 15 post-transduction, we sorted A375 and HT29 cells for CD4 expression levels, and HT29 for CD97 (ADGRE5). On day 19 we sorted both A375 and HT29 for CD274, and A375 cells for CD26 (DPP4). For each sort, we collected the top 1% and bottom 5% of the gene expression within the cell population. After sample processing and sequencing, we calculated the fold change between the log-normalized read counts of guides (LFC) in the high and low expressing populations, and z-scored these values relative to non-targeting control guides. The quasi-replicates were generally poorly-correlated (Supplementary Figure 1c), likely reflecting few true hits and noise associated with flow cytometry, especially relative to viability screens[29]. To mitigate false positives, we took the minimum z-score for each guide across the two dCas12a vectors instead of the average.

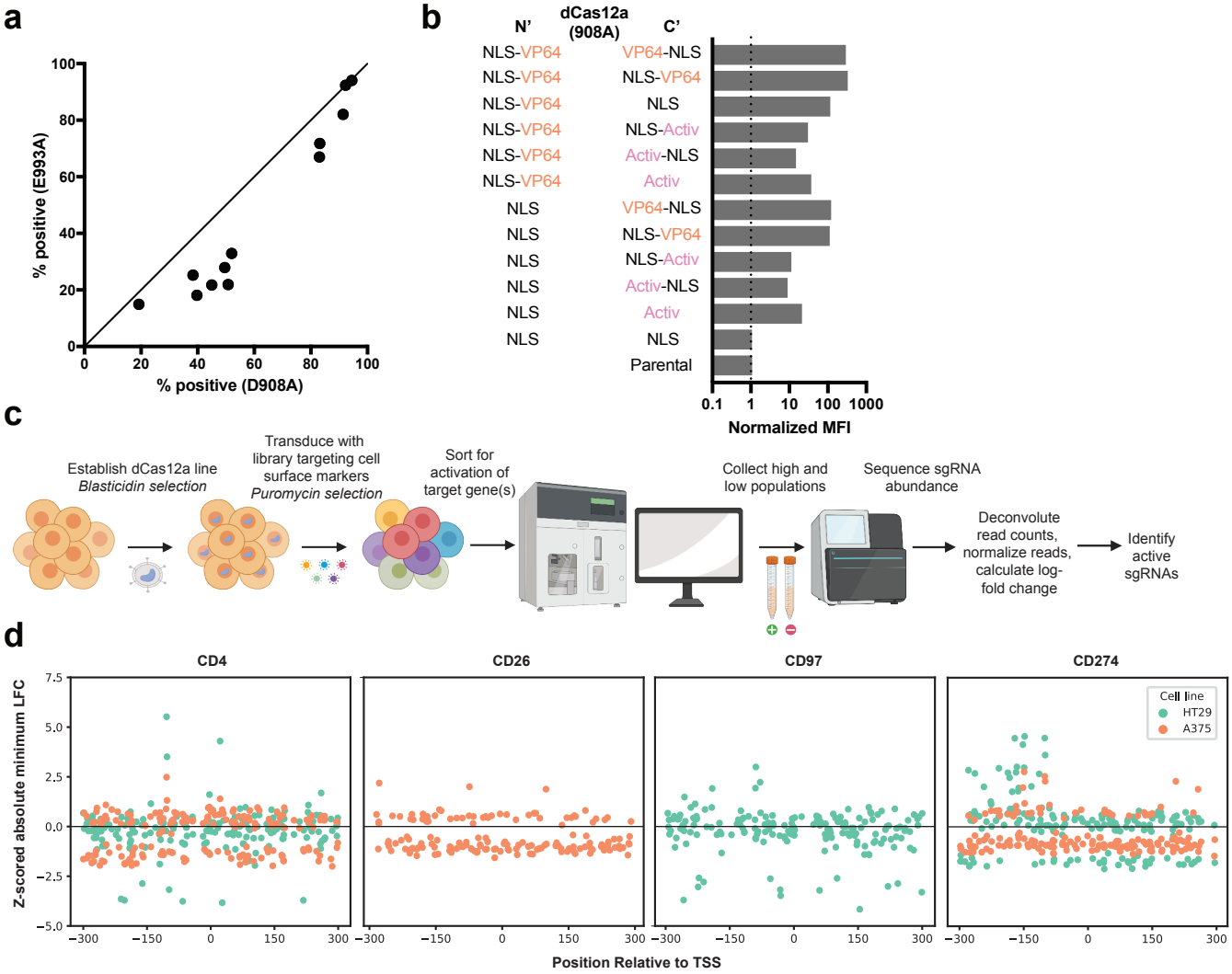

Figure 1. Evaluation of existing Cas12a CRISPRa technologies. A) Comparison of CRISPRa constructs employing two different nuclease-deactivating mutations of Cas12a. Activation was measured by the percentage of cells expressing CD4 five days after transduction. B) CD4 mean fluorescence intensity (MFI) normalized to baseline expression shown for 12 CRISPRa construct variants employing combinations of TADs directly tethered to dCas12a (D908A). C) Schematic depicting overview of the flow cytometry-based tiling screen performed to identify additional active Cas12a CRISPRa guides. D) Z-scores of the absolute minimum LFC for each guide across technological replicates are plotted by the location of the guide target site relative to the transcription start site (TSS) for CD4, CD26, CD97, and CD274.

127 We saw stronger enrichment of guides screened in HT29 cells, and noted that guide activity
128 varied by gene and by cell line throughout the region [-300 to +300] relative to the annotated
129 TSS (Figure 1d). Notably, the most enriched CD4-targeting guide identified in this screen was
130 the same guide that was most enriched in the initial CD4-targeting screen (Supplementary
131 Figure 1a). Active guides were rare, with only 1.1 - 9.4% of guides in the [-300 to +300] window
132 enriching with a z-score >2 in HT29 cells and 0.5 - 2.3 % in A375 cells. Further optimization of
133 this system is thus required before Cas12a CRISPRa can be implemented broadly for genetic
134 screens.

135 *Nanobody recruitment improves CRISPRa activity*

136 We next attempted to improve Cas12a CRISPRa potency and consistency with a TAD-
137 recruitment approach. Many groups have shown increased levels of activation with dCas9 using
138 recruitment-based systems, such as SAM and Suntag, which increase the local concentration of
139 TADs and afford more spatial flexibility[8,9]. The SAM system has been widely used for activation
140 purposes, including in genome-wide studies, but it does not translate readily to Cas12a
141 technology, as the DR sequence, functionally analogous to the tracrRNA, is much less
142 amenable to modification. We opted for a nanobody-based system to recruit TADs to dCas12a,
143 employing the ALFA tag, a 13 amino acid sequence, and the 14 kDa ALFA-nanobody to
144 colocalize linked proteins with high binding affinity[30]. This approach is conceptually similar to the
145 Suntag system, but with the added benefit of a smaller size, as the Suntag scFv-GCN4 is 26
146 kDa[9]. Additionally, both the ALFA tag and nanobody are entirely artificial sequences, ensuring
147 that they do not have endogenous targets in commonly studied organisms, including human and
148 mouse.
149
150 We engineered two sets of CRISPRa vectors with a) dCas12a linked to one or more ALFA tags
151 (hereafter, 'tag') and b) an ALFA nanobody (hereafter, 'nanobody') linked to one or more TADs
152 (Figure 2a). The latter vectors also contain the two CD4-targeting guides identified above. We
153 assembled five vectors with either 1, 3, or 5 tags in tandem on the N-terminus (N') of dCas12a
154 or 1 or 3 tags on the C-terminus (C'), as well as three additional vectors with either the VP64,
155 Activ, or p65 TAD linked to the nanobody. The 15 combinations of these vectors were tested in
156 three cell lines: HT29, A375, and HCC2429. We observed a range of CRISPRa activity across
157 cell lines and vector combinations, with HT29 showing the highest levels of CD4 activation
158 (Figure 2b). The N' 5x tag consistently outperformed 1x and 3x tag in all three cell lines.
159 Additionally, the N' 5x tag substantially outperformed C' 3x tag in two of three cell lines. We then
160 generated a C' 5x tag construct to compare to the N' 5x tag and found the N-terminal location to
161 be preferable across the three TADs tested (Supplementary Figure 2a). We again saw that Activ
162 induced minimal levels of CD4 activation, while VP64 and p65 both activated CD4 under several
163 conditions (Figure 2b).
164
165 Contemporaneous with the above experiments, we varied the number and location of the TADs
166 within the nanobody vector. We assembled 12 nanobody constructs containing the CD4 guides
167 and various configurations of the VP64, Activ, and p65 TADs. We tested these when paired with
168 three dCas12a vectors with a C' 3x tag with either VP64, p65, or no TAD tethered to the N-
169 terminus. We assessed these 36 combinations in HT29 cells and saw a wide range of activity,

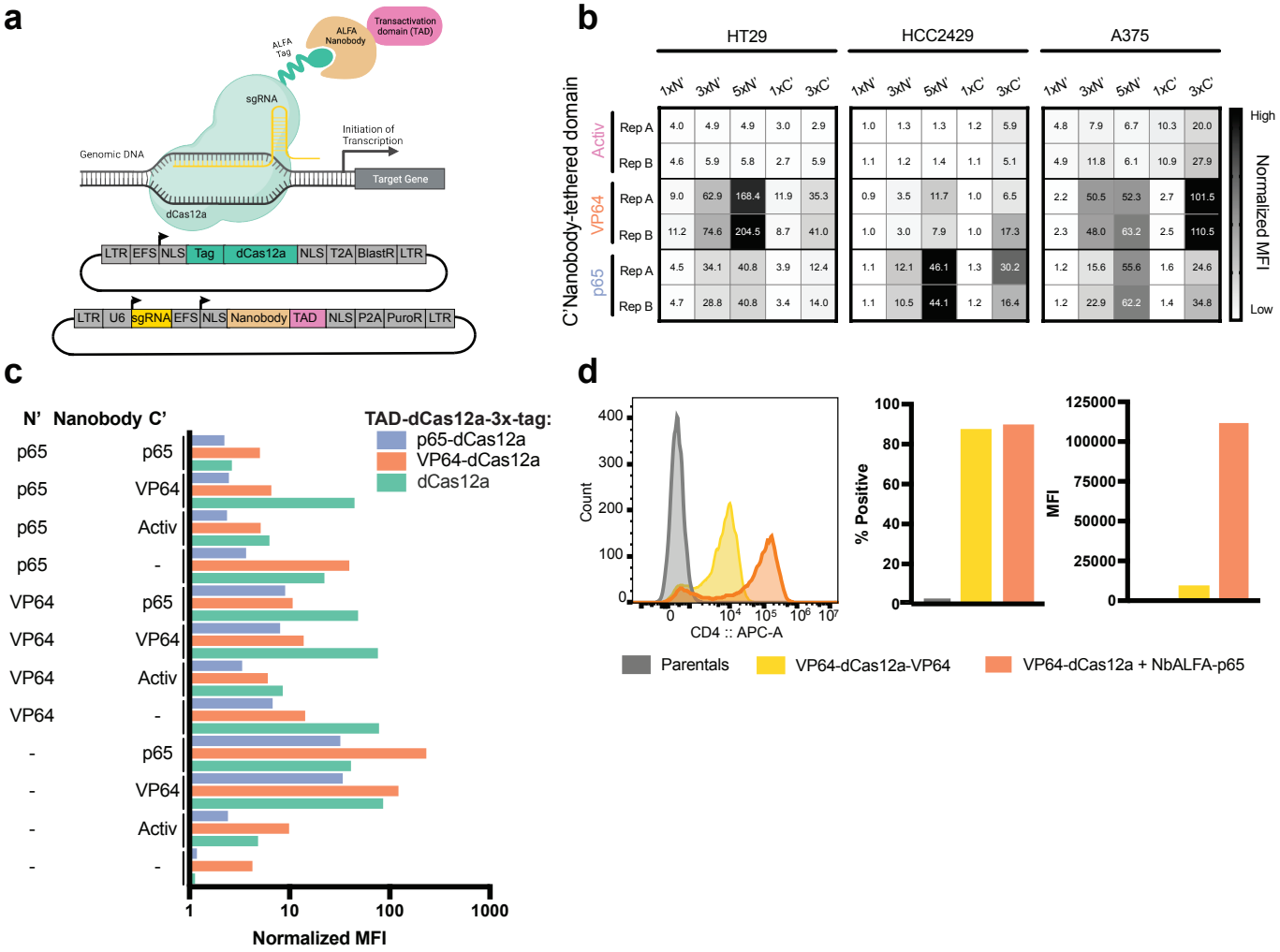

Figure 2. Nanobody recruitment improves CRISPRa activity. A) Schematic representing dCas12a nanobody-based recruitment of the transactivation domain (top). Plasmid maps depicting one vector containing the ALFA tag fused to dCas12a and a second vector containing the ALFA nanobody, TAD, and targeting guide (bottom). B) Heatmaps displaying comparative performance between the p65, VP64, and Activ TADs when recruited via nanobody to dCas12a harboring increasing numbers of ALFA tags (1x, 3x, 5x) at either the N- or C-terminus (N', C'). Experiments conducted in HT29, HCC2429, and A375 cell lines. Color scale reflects levels of normalized MFI of CD4 expression within each cell line. C) Barplot illustrating combinatorial effects emerging from the direct tethering of TADs to the N-terminus of dCas12a and nanobody-based recruitment of varying TAD configurations to the N and/or C-termini. X-axis shows normalized MFI values of CD4 expression on a log10 scale. D) Comparison of top-performers from the direct tethering-based and nanobody-based TAD recruitment approaches. Histogram shows the distribution of fluorescence peaks (left); barplots illustrate the percentage of cells expressing CD4 (middle), and CD4 MFI values (right).

170 with normalized MFI ranging from 1 to 226 fold-activation. We observed that nanobody vectors
171 with only one TAD on the C' terminus generally performed better than nanobody vectors with
172 TADs on both the N' and C' termini. Further, nanobody-VP64 performed best when paired with
173 dCas12a and VP64-dCas12a, while nanobody-p65 performed best with VP64-dCas12a. Finally,
174 nanobody-p65 led to the highest average activation of CD4 across all three dCas12a vectors
175 when compared to the 11 other nanobody configurations, and we identified the nanobody-p65 +
176 VP64-dCas12a-3x-tag combination as the top performer (Figure 2c). We then compared this
177 combination to the best direct-tether vector, VP64-dCas12a-VP64 (Figure 1b). We observed
178 that both approaches led to >85% of cells with CD4 expression, but the nanobody approach led
179 to a 226 fold-increase in MFI, compared to 16.9 for direct tethering, a 13-fold difference (Figure
180 2d).
181
182 Finally, we tested three additional nanobody vectors that deliver the bipartite TAD p65-HSF1,
183 used in the SAM system, either alone or in addition to VP64 or p65. We directly compared the
184 performance of the previous top activator, nanobody-p65, to these three new vectors when
185 paired with VP64-dCas12a-3x-tag in HT29 cells and saw a small increase in normalized CD4
186 MFI with recruitment of nanobody-p65-HSF1 compared to nanobody-p65 (Supplementary
187 Figure 2b). We also assessed the effect of including an additional NLS on the C-terminus of
188 nanobody-p65, and observed that the addition of a second NLS modestly improved CRISPRa
189 efficiency (Supplementary Figure 2c).
190
191 In this series of experiments, we tested several dozen combinations of ALFA tag positions and
192 numbers, TADs directly tethered to dCas12a, and combinations of TADs recruited via the ALFA
193 nanobody. We note that we did not test all possible combinations, and these assayed relied
194 entirely on the activation of one gene, CD4. We chose to move forward with a single dCas12a
195 vector, 5x-tag-dCas12a-VP64 (Supplementary Figure 2a), as well as three nanobody vectors –
196 nanobody-VP64 (Figure 2c), nanobody-p65 (Figure 2c), and nanobody-p65-HSF1
197 (Supplementary Figure 2b) – for additional experiments to understand how these results
198 generalize across other target genes and cell types.

199 *Effective multiplexing with nanobody-based systems*

200 Returning to the tiling screens described above (Figure 1), we generated vectors to activate
201 CD4, CD97, CD26, and CD274. For each gene, we selected three guides that showed activity in
202 at least one cell line, ensuring that the target sites for the selected guides did not overlap. We
203 multiplexed all three guides targeting a single gene into one construct, and for each, assembled
204 three vectors containing the nanobody and either VP64, p65, or p65-HSF1, for a total of 12
205 unique vectors (Figure 3a). We then transduced each vector in duplicate into HT29, A375 and
206 HCC2429 cells stably expressing 5x-tag-dCas12a-VP64 and selected with puromycin for five
207 days. We observed a severe growth effect with the nanobody-p65-HSF1 constructs in A375
208 cells and thus eliminated them from the remainder of the experiment.
209
210 Seven days after guide transduction, we assessed activity by flow cytometry. We observed
211 varied activation across each gene, cell line, and nanobody-TAD vector (Figure 3a); this mirrors
212 prior results with Cas9-based activation, that there is no completely generalizable CRISPRa

technology[16]. For example, CD26 expression was activated in HT29 cells, with a maximum fold-increase in MFI of 16.4, but little activation was seen in either A375 or HCC2429 cells. For the remaining three genes, fold-increase in activation ranged from 33.3 to 148.4 in HT29, 7.9 to 116.3 in A375, and 12.4 to 149.8 in HCC2429, while the corresponding percent-positive populations ranged from 97.8% to 100%, 60.9% to 95.6%, and 36.4% to 95.6%, respectively (Supplementary Data 2). Whereas the nanobody-p65 vector consistently achieved the highest level of activation across all genes in A375 and HCC2429 cells, this trend did not hold for HT29. Instead, we observed that the highest expression of each gene was achieved with a different TAD: p65-HSF1 for CD4 and CD274; p65 for CD26; and VP64 for CD97. Although no single nanobody-TAD vector consistently led to highest activity, all TADs, genes, and cell lines showed activation in at least one setting (Figure 3a).

Next, we tested the combinatorial capabilities of these nanobody-based Cas12a activation approaches by generating three new guide cassettes that contained one guide for each of the four cell surface genes (Figure 3b). We then paired the guide cassettes with the three nanobody-TAD vectors as before (VP64, p65, and p65-HSF1) in the same cell lines (HT29, A375, HCC2429) expressing 5x-tag-dCas12a-VP64. We analyzed all four surface markers via flow cytometry nine days following transduction and puromycin selection. Once again, A375 cells with the p65-HSF1 TAD died, suggesting that this cell line may be particularly sensitive to the expression of HSF1 and that this TAD may not be suitable for all-purpose CRISPRa approaches, at least with the strong EFS promoter used for TAD expression in this experiment.

In HT29 cells, the top construct activated all four markers, with average fold-increase in MFI ranging from 7.7 - 608.4 when paired with the p65-TAD. We saw the strongest activation of CD4, CD26, and CD274 with the guide cassette containing the top guides, while the strongest activation of CD97 was achieved with the cassette containing its third-ranked guide. As we had observed when targeting each gene individually, we were unable to achieve CD26 activation in A375 or HCC2429 with any of the guide combinations (Figure 3b). Although the TAD domain that led to maximal activation varied by gene and by cell line, the nanobody-p65 construct showed the most generalizable activity.

We next sought to assess the specificity of the nanobody-based recruitment approach. We performed bulk RNA sequencing (RNA-seq) on MelJuSo cells expressing 5x-tag-dCas12a-VP64 and nanobody-p65 or nanobody-VP64 with or without the cassette containing three CD4-targeting guides described above (Supplementary Figure 3a). We used DESeq2 to perform differential gene analysis and shrunken LFC to measure differences in activity, as this metric allows for the shrinkage of LFC estimates towards zero for genes with low normalized read counts[31,32]. We noted that CD4 was the most significantly upregulated gene in both comparisons, indicating good on-target efficacy for both CRISPRa systems (Figure 3c). In contrast, CD4 showed no evidence of upregulation in the absence of guides (Supplementary Figure 3b). To gain insight into the relationship between gene expression and proximity to the target site, we examined all the genes within the +/- 500 kb region surrounding CD4, observing minimal differential expression of nearby genes (Supplementary Figure 3c). Overall, these results show that these CRISPRa approaches have reasonable specificity.

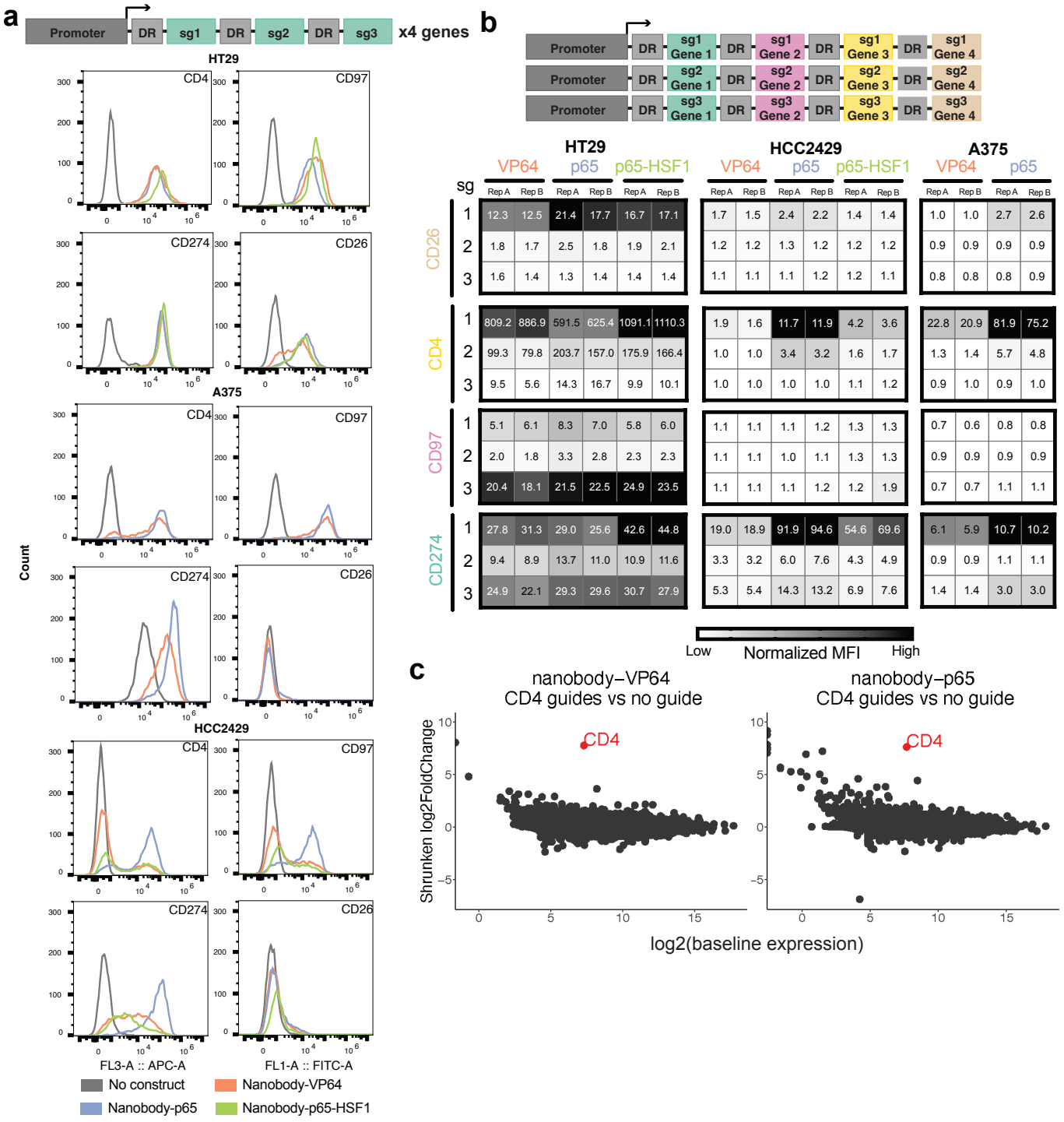

Figure 3. Effective multiplexing with a nanobody-based system. A) Schematic depicting single-gene targeting guide cassette architecture (top). Histograms show expression levels of CD4 (APC), CD274 (APC), CD97 (FITC), and CD26 (FITC) in HT29, A375, and HCC2429 cells expressing 5x-tag-dCas12a-VP64 when targeted individually by three guides per gene paired with nanobody-VP64, nanobody-p65, or nanobody-p65-HSF1 (bottom). Data from one representative replicate shown; data for all replicates is included in Supplementary Data 2. B) Schematic depicting multiplexed targeting guide cassette architecture (top). Heatmaps of normalized MFI values for CD26, CD4, CD97, and CD274 in HT29, A375, and HCC2429 cells expressing 5x-tag-dCas12a-VP64 when targeted simultaneously by one guide per gene paired with nanobody-VP64, nanobody-p65, or nanobody-p65-HSF1. MFI values were normalized to basal expression within each cell line/gene combination, as is the color scale (bottom). C) Comparison of RNA expression levels across samples expressing 5x-tag-dCas12a-VP64 and either nanobody-VP64 or nanobody-p65 with or without three CD4-targeting guides. Shrunken LFC in the CD4-targeting population is plotted against mean normalized read counts of all replicates for baseline expression (n = 3).

257 *Genome-wide activation with Cas12a*

258 To assess how well these technologies extrapolate to additional gene targets, we designed a
259 genome-wide library by varying several different design parameters. First, guide sequences
260 were generated to target either a window spanning [-300 to 0] or [-450 to 375] nucleotides
261 relative to the annotated TSS (hereafter respectively referred to as “narrow” or “wide”). Six
262 guides were chosen per targeting window and then divided into Set A and Set B, with three
263 guides per cassette, with a spacing requirement of 40 or 80 nucleotides between guides for the
264 narrow and wide windows, respectively. This resulted in 4 constructs per gene, and each sub-
265 library was cloned into two nanobody vectors containing either the p65 or VP64 TAD (Figure
266 4a).

267 Each library was screened in duplicate in MelJuSo cells stably expressing 5x-tag-dCas12a-
268 VP64 at a coverage of 1,000 cells per construct. Seven days post-transduction, each screen
269 was split into two conditions: a viability arm and a modifier arm with the MEK-inhibitor
270 selumetinib to allow for comparisons to a previous activation screen using a Cas9 CRISPRa
271 library[33]. Samples were collected at day 21, then guides were retrieved by PCR and sequenced.
272 LFC values for the viability arm were derived by comparing the day 21 sample to sequencing of
273 the plasmid DNA library (pDNA), while the modifier arm was assessed by comparing day 21
274 samples with and without selumetinib. Replicate Pearson correlation ranged from (0.75 - 0.85)
275 for the viability comparison and (0.25 - 0.6) for selumetinib; lower correlations are expected for
276 drug modifier screens, due to relatively fewer genes likely involved in the phenotype and noise
277 associated with strong positive selection.

278 To identify scoring genes, we averaged the LFC values of the four constructs for each gene and
279 then calculated gene-level z-scores relative to constructs targeting olfactory receptors (OR
280 genes). The p65 and VP64 TADs performed similarly, with a Pearson correlation of 0.78 in the
281 viability arm and 0.57 in the selumetinib arm (Figure 4b). Using a cutoff of |z-score| > 2, we
282 identified 529 genes that scored across the selumetinib and viability arms with either VP64, p65,
283 or both, with 53 more hits identified with p65 than with VP64 at that threshold. We averaged the
284 z-scores across the two TADs for subsequent analyses.

285 Examining the viability arm, 208 genes scored with a z-score < -2 as negatively impacting cell
286 proliferation. Three of the top five most-depleted genes were the cyclin-dependent kinase
287 inhibitors CDKN1A, CDKN1C, and CDKN2C, which are well-established as growth-inhibitors
288 based on their action on critical cell cycle components (Figure 4b). Importantly, CDKN2A (which
289 encodes p16INK4a and p14ARF) is deleted in MelJuSo cells[34] and did not score, with a z-score
290 of -0.1 (Supplementary Figure 4a). Other top hits include the transcription factor JUNB, a
291 member of the AP-1 family of transcription factors; MAP3K11, a Jun N-terminal kinase whose
292 overexpression has previously been shown to inhibit the proliferation of B cells[35]; and PRDM1
293 (also known as BLIMP-1), a critical transcription factor in B cell, T cell, and myeloid lineages
294 (Figure 4b). Few genes scored as enhancing proliferation; only 7 genes scored with a z-score
295 >2 and none scored with a z-score >3. That there are substantially more negative regulators of
296 proliferation upon activation mirrors results seen previously with ORF-based viability screens,
297 which identified 103 STOP genes and only 3 GO genes that scored in common across three cell

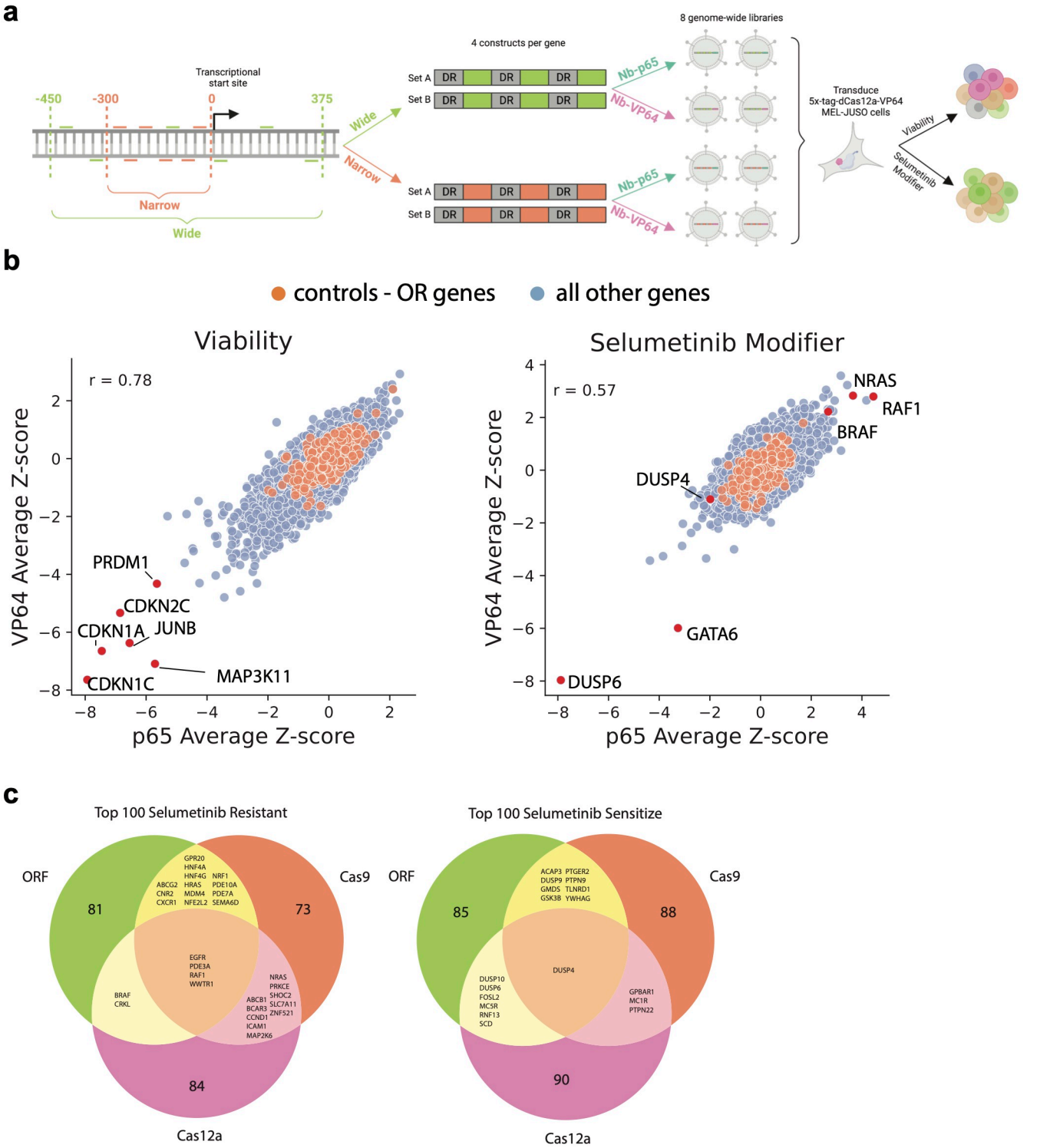

Figure 4. Development of Cas12a genome-wide activation libraries. A) Schematic representing dCas12a screening approach encompassing the “wide” [-450 to 375] and “narrow” [-300 to 0] targeting windows relative to the annotated TSS; each gene is targeted by 6 guides (3 in Set A and 3 in Set B). Both sets for the two targeting windows were tested with the p65 and VP64 nanobody approach. B) Scatter plot comparing the p65 and VP64 nanobody approaches in the viability arm (left) and selumetinib drug arm (right), with select genes highlighted. C) Venn diagrams showing overlapping top 100 genes between the dCas9, dCas12a, and ORF selumetinib modifier screens for resistance and sensitization.

298 lines[36].

299 Examining the selumetinib modifier screen, the top sensitizing hit was the phosphatase DUSP6,
300 which aligns with a recent study showing that DUSP6 knockout (along with its paralog, DUSP4)
301 hyperactives the MAPK pathway[37]. Activation of DUSP6, then, would be expected to
302 downregulate the pathway and render the cells more sensitive to further inhibition by
303 selumetinib. Another sensitizing hit was GATA6, which has been shown to be positively
304 regulated by Erk phosphorylation[38], a result less obviously expected, but suggests the existence
305 of a feedback loop or other regulatory logic downstream of activated Erk. On the resistance
306 side, RAF1 (rank 1), NRAS (rank 5), and BRAF (rank 13) are all upstream of MEK and thus their
307 overexpression would be expected to buffer the effects of selumetinib (Figure 4b). Interestingly,
308 neither gene encoding a MEK paralog scored (MAP2K1, z-score 0.3; MAP2K2, z-score -0.5) nor
309 did ERK paralogs (MAPK1, z-score 0.5; MAPK3, z-score 0.1). Whether these represent false
310 negatives of the CRISPRa approach or a true reflection of pathway dynamics would require
311 further testing. Many other top-scoring genes, however, have no clear connection to the MAPK
312 pathway and thus represent a starting point for future studies of signaling and regulation.

313 Gold-standard reference sets of essential and nonessential genes[39] have been critical to
314 benchmark the performance of CRISPR knockout and interference libraries, however, no such
315 parallel ground truth exists for genes expected to score in a viability screen upon
316 overexpression. Comparison to open reading frame (ORF) libraries represents a reasonable
317 starting point, although there are substantive differences between this approach and CRISPRa;
318 for example, the former will not recapitulate native splicing patterns or UTR-mediated regulation.
319 Nevertheless, a gene that scores by both technologies is quite unlikely to represent a dual false
320 positive, and thus ORF screens can inform assessment of CRISPRa approaches. We thus
321 conducted both viability and selumetinib modifier screens with a genome-scale ORF library[40,41]
322 in MelJuSo cells as described above, harvesting cells on day 4 rather than relying on the pDNA
323 to represent starting library abundance due to the varied packaging efficiency of differently-sized
324 ORFs. LFC values for the viability arm were derived by comparing the day 21 sample to the day
325 4 sample, and the modifier arm was assessed by comparing day 21 samples with and without
326 selumetinib. Pearson correlation across replicates were 0.66 for the viability arm and 0.44 for
327 the selumetinib arm. (Supplementary Figure 4b).

328 We had also previously conducted screens in this model with the Cas9-based Calabrese
329 library[33]. 10,351 genes were screened with all three modalities – ORF, Cas9, Cas12a – and we
330 examined the overlap of the top 100 hits from each (Figure 4c, Supplementary Figure 4c). In the
331 selumetinib treatment arm, four genes scored as resistance hits across all screens, RAF1,
332 EGFR, PDE3A, and WWTR1 (more commonly known as the transcriptional coactivator TAZ).
333 For selumetinib sensitivity, DUSP4 scored with all three approaches, while 17 genes scored in
334 two of the three, including DUSP6 and DUSP10, which scored with both ORF and Cas12a, and
335 likely represent false negatives of the Cas9 screen; conversely, DUSP9 did not score with
336 Cas12a but did with Cas9 and ORF (Figure 4c). Overall, however, many genes scored uniquely
337 to one modality. A systematic exploration of the features leading to false negatives with each
338 technology is an important future direction, and the candidate genes identified here will be a
339 valuable resource for such studies.

340 *Validation of screen hits to learn rules for effective targeting*

341 To understand design principles for Cas12a-based CRISPRa guides, we constructed a
342 validation library, including all genes that scored as hits (|z-score| > 2) with either VP64 or p65
343 in the viability and selumetinib screens (n = 529, Supplementary Figure 5a). We included the 3-
344 guides-per-cassette designs used in the primary screen as well as all individual guides targeting
345 these genes. For genes that reached the hit threshold with both TADs (n = 142), we tested all
346 shuffled orders of the 3-guides-per-cassette design, as well as all pairwise combinations
347 (Supplementary Figure 5a).
348
349 This library was cloned into two nanobody vectors, containing either the p65 or VP64 TAD.
350 Each library was screened in duplicate in MelJuSo cells stably expressing 5x-tag-dCas12a-
351 VP64 according to the same timeline as the primary screen. LFCs were calculated as described
352 above, then construct level z-scores were calculated relative to intergenic controls. We first
353 examined the reproducibility of the secondary screen by comparing the z-scores of the original
354 triple-guide constructs in the primary and secondary screens and saw a Pearson correlation of
355 0.82 (Figure 5a). Further, replicates and TADs were well correlated (Supplementary Figure 5b),
356 so we averaged the z-score between the two TADs for all subsequent analyses. We then
357 selected a set of highest confidence genes, defined as those that scored (|z-score| > 2) with
358 both TADs in both the primary screen and the secondary screen, consisting of 9 genes from the
359 viability arm and 11 from the selumetinib arm.
360
361 We examined the efficacy of targeting with single, dual, or triple guide constructs to assess the
362 effectiveness of higher-order multiplexing using the highest confidence gene set and found that
363 triple guide constructs performed the best (Figure 5b, Supplementary Figure 5c). Additionally,
364 we found that the best performing single guide is much more predictive of the performance of
365 dual guide constructs than the worst performing single guide (Figure 5c). We then sought to
366 understand whether the order of guides impacts performance. Using all shuffled triple-guide
367 constructs, we determined pairwise Pearson correlation for all permutations and found the
368 median correlation to be 0.81 for viability and 0.84 for selumetinib, demonstrating consistent
369 construct performance regardless of guide order (Supplementary Figure 5d).
370
371 Previously, we developed an on-target scoring approach for Cas12a based on activity in
372 knockout screens, enPAM+GB[19], and we wanted to assess the predictive value of this score for
373 CRISPRa. We thus binned single guides into high (|z-score| > 2), medium (|z-score| <= 2 and
374 |z-score| > 1), and low (|z-score| <= 1) activity bins and observed that highly active guides
375 tended to have the highest on-target efficacy scores (Figure 5d). Additionally, we examined
376 guide activity as a function of location relative to the TSS and observed more activity in the
377 region upstream of the TSS (Figure 5e), as has been seen previously with Cas9-based
378 CRISPRa[33,42]. Finally, we sought to explore the interaction between enPAM+GB and the TSS
379 window. We established a threshold based on the 25th percentile of enPAM+GB scores for
380 highly-active guides (enPAM+GB > 0.76), defined the optimal TSS window as 200 to 100
381 nucleotides upstream of the TSS, and created 4 bins based on these cutoffs. We observed that
382 56% of guides showed high activity in the bin with high enPAM+GB scores in the optimal TSS

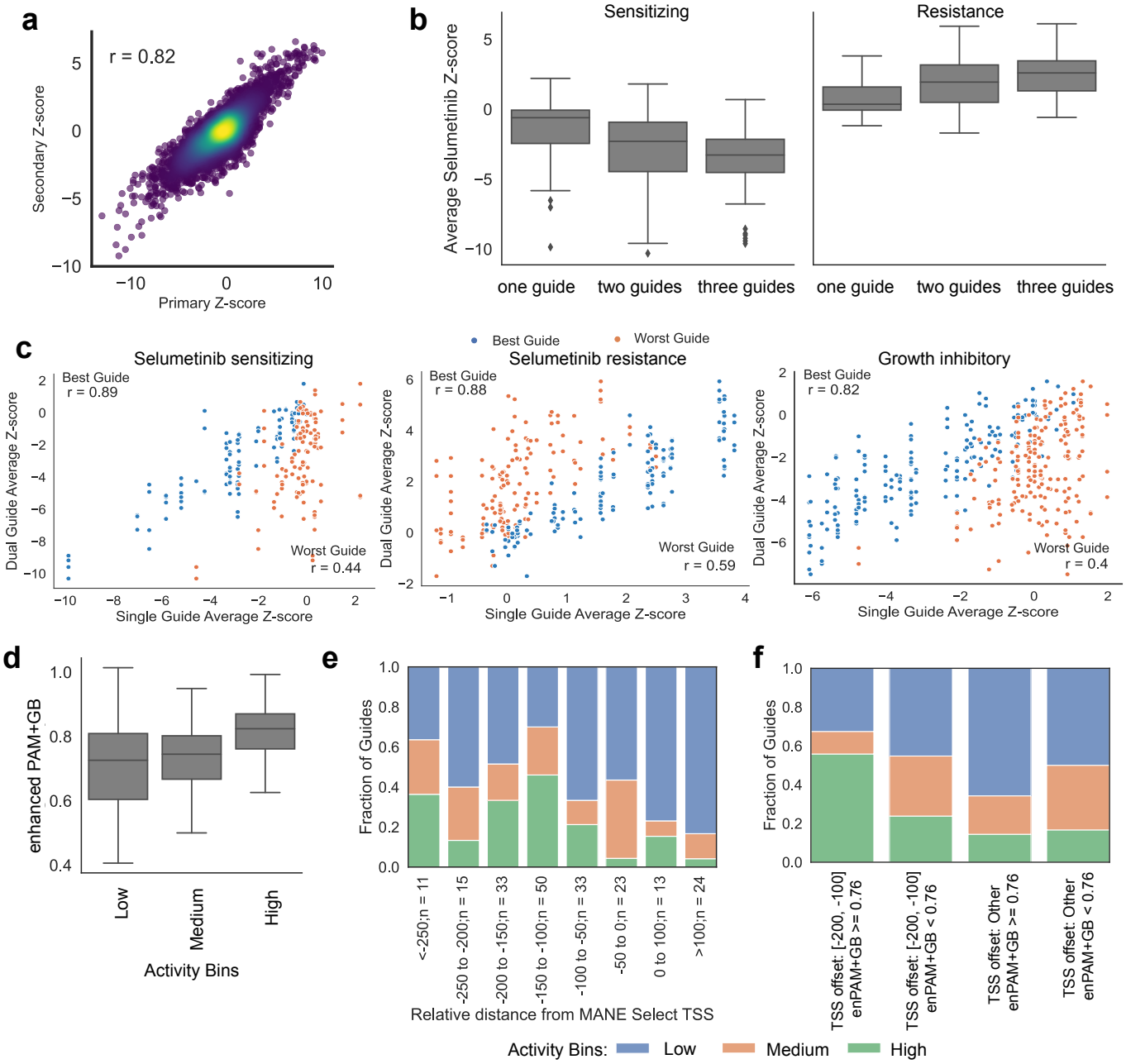

Figure 5. Validation of primary screen hits to learn on-rules for effective targeting. A) Scatterplot of z-scores comparing all triple-guide constructs in both primary and secondary screens. Each triple-guide construct has z-scores calculated in four screen arms: VP64 viability, VP64 selumetinib, p65 viability, p65 selumetinib (n = 8416 constructs). B) Comparison of z-score distributions for single, dual, or triple-guide constructs targeting highest confidence genes in the selumetnib arm: sensitizing genes (constructs = 291, left) and resistant genes (constructs = 346, right). Boxes show the quartiles (Q1 and Q3) as minima and maxima and the center represents the median; whiskers show 1.5 times the interquartile range (Q1 - 1.5*IQR and Q3 + 1.5*IQR). C) Scatterplots of z-score between dual-guide and single-guides targeting highest confidence selumetinib sensitizing genes (number of dual guides = 240, left), selumetinib resistant genes (number of dual guides = 286, middle), and growth-inhibitory genes (number of dual guides = 382, right). Pearson correlations of z-scores between dual-guides and best performing single guides and worst performing single guides are highlighted in the upper left and lower right corners, respectively. D) enPAM+GB scores for single-guide constructs, binned by z-score. There are 109 guides in the low active bin (|z-score| <= 1), 42 guides in the median active bin (1 < |z-score| <= 2), and 51 guides in the highly active bin (|z-score| > 2). E) Fraction of guides in each activity bin for single-guide constructs targeting the high confidence gene set relative to MANE select TSS. F) Fraction of guides in each activity bin for single-guide constructs targeting the high confidence gene set relative to MANE select TSS and enPAM+GB.

383 window, compared to 17% across the other three bins (Figure 5f). This guidance on guide
384 selection, coupled with the observation that a multi-guide construct largely mirrors the
385 performance of the best-performing guide, enables the design of CRISPRa constructs that are
386 likely to be effective.

387 DISCUSSION

388 Here we develop Cas12a for large scale CRISPRa screens. We compare the performance of
389 multiple activation approaches by linking the Cas protein to one or more commonly-used TADs
390 and show that a recruitment strategy with the ALFA nanobody and its complimentary ALFA tag
391 enables a high fraction of cells to overpress target genes when delivered by lentivirus, a
392 prerequisite for pooled genetic screens. We then leverage the advantages of Cas12a over Cas9
393 to readily multiplex guides in a compact cassette and activate several genes simultaneously.
394 Finally, we expand our understanding of Cas12a CRISPRa guide design considerations by
395 screening a genome-wide library.
396
397 Our findings highlight that there is still much to be learned about effective approaches for
398 CRISPRa, and that there is not, as yet, a one-size-fits-all approach. For example, reagents that
399 effectively activated CD97 in HT29 cells failed to do so in HCC2429 and A375 cells. Such
400 observations are not limited to Cas12a-based approaches, and have been well-documented in
401 prior studies with Cas9[16]. This impression gleaned from small-scale study of individual genes is
402 dramatically reinforced by the comparison of CRISPRa to ORF overexpression at genome-
403 scale, as many genes scored only via the latter approach. While some of those hits may
404 represent false positives of the ORF screen, we suspect that the majority are false negatives of
405 CRISPRa technology. In addition to the trivial explanation of poor guide selection, biological
406 explanations include different TAD requirements across cell types, the presence of repressive
407 chromatin or DNA marks, and differences in nuclear location that impact CRISPRa potential,
408 among other explanations. These screens thus provide an important starting point to test these
409 hypotheses, for example, one could deeply screen these candidate genes with TADs other than
410 p65 and VP64, as well as domains that modulate the epigenome[43–45], and determine what
411 strategies, if any, can best recoup these false negatives of current CRISPRa approaches.
412
413 Several future directions are immediately enabled by the results and reagents described here,
414 especially given the multiplexing capabilities of Cas12a. First, for genome-wide screens focused
415 on individual genes, the false negative rate can be mitigated by targeting the same gene with
416 multiple guides in the same vector, and we provide guidance on effective guide selection. The
417 technology described here should likewise easily extend to combinatorial screens, such as
418 activating multiple genes at their respective promoters, an approach that is extraordinarily useful
419 to engineer cell types of interest and understand cell fate decisions. Further, scalable
420 combinatorial screens can enable dissection of the regulatory logic of the non-coding genome,
421 by jointly targeting potential enhancer elements and putative promoter targets[16,46]. In sum, we
422 have demonstrated methods for implementing Cas12a-based CRISPRa at scale in human cells.

423 METHODS

424 **Vectors**
425 pRDA_763 (Addgene #201156): EFS promoter expresses NLS, 5xALFA tag, dEnAsCas12a,
426 NLS; T2A site provides blasticidin resistance.
427 pRDA_816 (Addgene #201157): EFS promoter expresses NLS, 5xALFA tag, dEnAsCas12a,
428 VP64, NLS; T2A site provides blasticidin resistance.
429 pRDA_886 (Addgene #201162): U6 promoter expresses customizable Cas12a guide; EFS
430 promoter expresses NLS, NbALFA, VP64, NLS; P2A site provides puromycin resistance.
431 pRDA_887 (Addgene #201164): U6 promoter expresses customizable Cas12a guide; EFS
432 promoter expresses NLS, NbALFA, p65, NLS; P2A site provides puromycin resistance.
433 pRDA_888 (Addgene #201165): U6 promoter expresses customizable Cas12a guide; EFS
434 promoter expresses NLS, NbALFA, p65, HSF1, NLS; P2A site provides puromycin resistance.
435 pLX_317 (https://portals.broadinstitute.org/gpp/public/vector/details?vector=pLX_TRC317):
436 Destination vector for ORF sequences and associated barcodes.
437
438 **Cell lines and culture**
439 A375, A549, HCC2429, HT29, and MelJuSo cells were obtained from the Cancer Cell Line
440 Encyclopedia at the Broad Institute. HEK293Ts were obtained from ATCC (CRL-3216).
441
442 All cells regularly tested negative for mycoplasma contamination and were maintained in the
443 absence of antibiotics except during screens, flow cytometry-based experiments, and lentivirus
444 production, during which media was supplemented with 1% penicillin-streptomycin. Cells were
445 passaged every 2-4 days to maintain exponential growth and were kept in a humidity-controlled
446 37°C incubator with 5.0% CO2. Media conditions and doses of polybrene, puromycin, and
447 blasticidin were as follows, unless otherwise noted:
448
449 A375: RPMI + 10% fetal bovine serum (FBS); 1 µg/mL; 1 µg/mL; 5 µg/mL
450 A549: DMEM + 10% FBS; 1 µg/mL; 1.5 µg/mL; 5 µg/mL
451 HCC2429: RPMI + 10% FBS; 4 µg/mL; 2 µg/mL; 8 µg/mL
452 HT29: DMEM + 10% FBS, 1 µg/mL; 2 µg/mL; 8 µg/mL
453 MelJuSo: RPMI + 10% FBS; 4 µg/mL; 1 µg/mL; 4 µg/mL
454 HEK293T: DMEM + 10% heat-inactivated FBS; N/A; N/A; N/A
455
456 **CD4 CRISPRa library design**
457 10 CD4-targeting guides and 20 guides targeting 20 individual olfactory receptor genes were
458 selected using the guide design tool CRISPick. An additional 29 guides targeting CD45 were
459 also selected, but these were not assessed in the manuscript. These guides were pre-filtered to
460 exclude BsmBI recognition sites or poly-T sequences. Each of the 59 guides was placed in the
461 first position and paired with all 58 remaining guides in the library at the second position, for a
462 total of n = 3,422 unique vectors. The wild-type DR and DR_v2 (TAATTTCTACTATCGTAGAT)
463 were used with the guides in the first and second position, respectively.
464
465 **Cell surface marker tiling library design**
466 Guide sequences for the tiling library were designed using sequence annotations from Ensembl
467 (GRCh38). CRISPick was used to select every possible guide (using an NNNN PAM) against
468 the longest annotated transcript for 17 genes: CD47, CD63, B2M, CD274, CD46, CD55, CD81,
469 CSTB, CD4, CD26, CD97, CD59, BSG, LDLR, LRRC8A, PIGA, and TFRC. We included guides
470 targeting the coding sequence, all guides for which the start was up to 30 nucleotides into the
471 intron and UTRs, and all guides targeting the window 0-300 bp upstream of the annotated TSS.
472 The library was filtered to exclude any guides with BsmBI recognition sites or TTTT sequences,

473 and guides were annotated to denote the CRISPR technologies with which they were
474 compatible (CRISPRko, CRISPRbe, CRISPRa and/or CRISPRi). Guides with >3 or >5 perfect
475 matches in the genome for CRISPRko/CRISPRbe or CRISPRa/CRISPRi technologies,
476 respectively, were also filtered out. Subsequently, a random 50% subsampling of the
477 CRISPRko/be guides was removed from the library to decrease library size. 700 positive and
478 negative control guides were added into the library, including 500 guides targeting intergenic
479 regions, 100 non-targeting guides, and 100 guides targeting essential splice sites, for a total
480 library size of n = 8,421.
481
482 **CRISPRa genome-wide library design**
483 Using CRISPick with sequence annotations from NCBI (GRCh38), we generated genome-wide
484 tiling design files with narrow or wide regions around the TSS. NCBI incorporates MANE select
485 annotation for TSS location. “Narrow” is defined as 300 upstream of TSS to TSS. “Wide” is
486 defined as 450 upstream to 375 downstream of TSS. We filtered 382,820 guides with NAs in
487 pick order and 10,000 or greater off-target sites for the narrow design and 1,129,916 guides for
488 wide design. After filtering, 1,688,088 guides and 19,272 genes remained in the narrow design
489 and 4,488,819 guides and 19,284 genes remained in the wide design. For each tiling genome-
490 wide design file, guides were sorted by pick order within each gene and selected with a
491 minimum spacing requirement of 40 nucleotides for the narrow design and 80 nucleotides for
492 the wide design. This procedure was first applied to select three guides per vector for Set A and
493 then repeated for Set B. There are 18,715 genes in narrow Set A, 18,715 genes in narrow Set
494 B, 18,580 genes in wide Set A, and 18,580 genes in wide Set B. Each set was then cloned into
495 the VP64 or p65 nanobody-TAD vectors.
496
497 **CRISPRa secondary screen library design**
498 The library consists of five parts. First, we identified the union of resistant hits (z-score >2) and
499 sensitizing hit (z-score <-2) across VP64 and p65 for the viability and selumetinib arms, which
500 totals 529 genes. We included each individual guide in these 529 genes as individual constructs
501 in the secondary screen, totaling 5423 constructs with one guide per construct (2 TSS windows
502 x 2 Sets(A/B) x 529 total hits x 3 guides - 925 duplicate guides). Second, we included the
503 original triple guide construct targeting each of these 529 hits, totaling 2116 constructs (2 TSS
504 windows x 2 Sets(A/B) x 529 total hits). Third, we identified the overlapping hits between VP64
505 and p65 in the selumetinib resistance, selumetinib sensitizing, viability resistance, and viability
506 sensitizing directions, which sum to 142 genes. We included all possible permutations of triple
507 guide constructs targeting these 142 genes, totaling 2840 constructs with three guides per
508 construct (2 TSS windows x 2 Sets(A/B) x 142 overlap hits x 5 permutations). Fourth, we
509 targeted all of the overlapping hits in all possible permutations of double guide constructs,
510 totaling 3408 constructs with two guides per construct (2 TSS windows x 2 Sets(A/B) x 142
511 overlap hits x 6 permutations). Lastly, we included 1000 intergenic controls with 334 single
512 guide controls, 333 double guide controls, and 333 triple guide controls. In total, the secondary
513 library contains 14,787 constructs, which were then cloned into the nanobody-VP64 and
514 nanobody-p65 vectors, resulting in a total of two secondary libraries.
515
516 **ORF library**
517 ORF screens used a pre-existing lentiviral ORF library consisting of 17,522 ORF constructs with
518 barcodes cloned into pLX_317 as described in ref.[34]
519
520 **Library production**
521 Oligonucleotide pools were synthesized by Genscript. BsmBI recognition sites were appended
522 to each guide sequence along with the appropriate overhang sequences (bold italic) for cloning

523 into the guide expression vectors, as well as primer sites to allow differential amplification of
524 subsets from the same synthesis pool. The final oligonucleotide sequence was thus: 5′-[forward
525 primer]CGTCTC***AAGAT***[guide RNA]TTTTTT***GAATC***GAGACG[reverse primer].
526
527 Primers were used to amplify individual subpools using 25 µL 2x NEBnext PCR master mix
528 (New England Biolabs), 2 µL of oligonucleotide pool (~40 ng), 5 µL of primer mix at a final
529 concentration of 0.5 µM, and 18 µL water. PCR cycling conditions: (1) 98°C for 30 seconds; (2)
530 53°C for 30 seconds; (3) 72°C for 30 seconds; (4) go to (1), x 24.
531
532 In cases where a library was divided into subsets, unique primers could be used for
533 amplification:
534
535 Primer Set; Forward Primer, 5′ – 3′; Reverse Primer, 5′ – 3′
536 1; GTGTAACCCGTAGGGCACCT; GTCGAAGGACTGCTCTCGAC
537 2; CAGCGCCAATGGGCTTTCGA; CGACAGGCTCTTAAGCGGCT
538 3; CTACAGGTACCGGTCCTGAG; CGGATCGTCACGCTAGGTAC
539 4; CGACGTTATGGATCGACGCC; AGGTGTCGCGGACTACTCAC
540
541 The resulting amplicons were PCR-purified (Qiagen) and cloned into the library vector via
542 Golden Gate cloning with Esp3I (Fisher Scientific) and T7 ligase (Epizyme); the library vector
543 was pre-digested with BsmBI (New England Biolabs). The ligation product was isopropanol
544 precipitated and electroporated into Stbl4 electrocompetent cells (Invitrogen) and grown at 30
545 °C for 16 h on agar with 100 µg/mL carbenicillin. Colonies were scraped and plasmid DNA
546 (pDNA) was prepared (HiSpeed Plasmid Maxi, Qiagen). To confirm library representation and
547 distribution, the pDNA was sequenced.
548
549 **Lentivirus production**
550 For small-scale virus production, the following procedure was used: 24 h before transfection,
551 HEK293T cells were seeded in 6-well dishes at a density of 1.5×10^6 cells per well in 2 mL of
552 DMEM + 10% heat-inactivated FBS. Transfection was performed using TransIT-LT1 (Mirus)
553 transfection reagent according to the manufacturer's protocol. Briefly, one solution of Opti-MEM
554 (Corning, 66.75 µL) and LT1 (8.25 µL) was combined with a DNA mixture of the packaging
555 plasmid pCMV_VSVG (Addgene 8454, 125 ng), psPAX2 (Addgene 12260, 1250 ng), and the
556 transfer vector (e.g., the library pool, 1250 ng). The solutions were incubated at room
557 temperature for 20–30 min, during which time media was changed on the HEK293T cells. After
558 this incubation, the transfection mixture was added dropwise to the surface of the HEK293T
559 cells, and the plates were centrifuged at 1000 g for 30 min at room temperature. Following
560 centrifugation, plates were transferred to a 37°C incubator for 6–8 h, after which the media was
561 removed and replaced with DMEM +10% FBS media supplemented with 1% BSA. Virus was
562 harvested 36 h after this media change.
563
564 A larger-scale procedure was used for pooled library production. 24 h before transfection, $18 \times$
565 10^6 HEK293T cells were seeded in a 175 cm^2 tissue culture flask and the transfection was
566 performed the same as for small-scale production using 6 mL of Opti-MEM, 305 µL of LT1, and
567 a DNA mixture of pCMV_VSVG (5 µg), psPAX2 (50 µg), and 40 µg of the transfer vector. Flasks
568 were transferred to a 37°C incubator for 6–8 h; after this, the media was aspirated and replaced
569 with BSA-supplemented media. Virus was harvested 36 h after this media change.
570
571 **Determination of antibiotic dose**

572 In order to determine an appropriate antibiotic dose for each cell line, cells were transduced with
573 the pRosetta or pRosetta_v2 lentivirus such that approximately 30% of cells were transduced
574 and therefore EGFP+. At least 1 day post-transduction, cells were seeded into 6-well dishes at
575 a range of antibiotic doses (e.g. from 0 µg/mL to 8 µg/mL of puromycin). The rate of antibiotic
576 selection at each dose was then monitored by performing flow cytometry for EGFP+ cells. For
577 each cell line, the antibiotic dose was chosen to be the lowest dose that led to at least 95%
578 EGFP+ cells after antibiotic treatment for 7 days (for puromycin) or 14 days (for blasticidin).
579
580 **Small molecule doses in pooled screens**
581 For genome-wide primary and secondary screens in MelJuSo cells, selumetinib (Selleckchem,
582 AZD6244) was diluted in DMSO and was screened at 1.5 µM.
583
584 **Determination of lentiviral titer**
585 To determine lentiviral titer for transductions, cell lines were transduced in 12-well plates with a
586 range of virus volumes (e.g. 0, 150, 300, 500, and 800 µL virus) with 3×10^6 cells per well in the
587 presence of polybrene. The plates were centrifuged at 640 x g for 2 h and were then transferred
588 to a 37°C incubator for 4–6 h. Each well was then trypsinized, and an equal number of cells
589 seeded into each of two wells of a 6-well dish. Two days post-transduction, puromycin was
590 added to one well out of the pair. After 5 days, both wells were counted for viability. A viral dose
591 resulting in 30–50% transduction efficiency, corresponding to an MOI of ~0.35–0.70, was used
592 for subsequent library screening.
593
594 **Derivation of stable cell lines**
595 In order to establish the dCas12a expressing cell line for the large-scale screens with the
596 genome-wide libraries, MelJuSo cells were transduced with pRDA_816 (5x-tag-dCas12a-VP64),
597 and successfully transduced cells were selected with blasticidin for a minimum of 2 weeks. Cells
598 were taken off blasticidin at least one passage before transduction with libraries.
599
600 **Pooled screens**
601 For pooled screens, cells were transduced in two biological replicates with the lentiviral library.
602 Transductions were performed at a low multiplicity of infection (MOI ~0.5), using enough cells to
603 achieve a representation of at least 1000 transduced cells per guide assuming a 20-40%
604 transduction efficiency. Cells were plated in polybrene-containing media with 3×10^6 cells per
605 well in a 12-well plate. Plates were centrifuged for 2 hours at 821 x g, after which 2 mL of media
606 was added to each well. Plates were then transferred to an incubator for 4-6 hours, after which
607 virus-containing media was removed and cells were pooled into flasks. Puromycin was added 2
608 days post-transduction and maintained for 5 days to ensure complete removal of non-
609 transduced cells. Upon puromycin removal, cells were split to any drug arms (each at a
610 representation of at least 1,000 cells per guide) and passaged on drug every 2-3 days for an
611 additional 2 weeks to allow guides to enrich or deplete; cell counts were taken at each passage
612 to monitor growth.
613
614 **Genomic DNA isolation and sequencing**
615 Genomic DNA (gDNA) was isolated using the KingFisher Flex Purification System with the Mag-
616 Bind® Blood & Tissue DNA HDQ Kit (Omega Bio-Tek). The gDNA concentrations were
617 quantitated by Qubit.
618
619 For PCR amplification, gDNA was divided into 100 µL reactions such that each well had at most
620 10 µg of gDNA. Plasmid DNA (pDNA) was also included at a maximum of 100 pg per well. Per
621 96-well plate, a master mix consisted of 150 µL DNA Polymerase (Titanium Taq; Takara), 1 mL
622 of 10x buffer, 800 µL of dNTPs (Takara), 50 µL of P5 stagger primer mix (stock at 100 µM

concentration), 500 µL of DMSO (if used), and water to bring the final volume to 4 mL. Each well consisted of 50 µL gDNA and water, 40 µL PCR master mix, and 10 µL of a uniquely barcoded P7 primer (stock at 5 µM concentration). PCR cycling conditions were as follows: (1) 95°C for 1 minute; (2) 94°C for 30 seconds; (3) 52.5°C for 30 seconds; (4) 72°C for 30 seconds; (5) go to (2), x 27; (6) 72°C for 10 minutes. PCR primers were synthesized at Integrated DNA Technologies (IDT). PCR products were purified with Agencourt AMPure XP SPRI beads according to manufacturer's instructions (Beckman Coulter, A63880), using a 1:1 ratio of beads to PCR product. Samples were sequenced on a HiSeq2500 HighOutput (Illumina) with a 5% spike-in of PhiX, using a custom oligo (oligo sequence: CTTGTGGAAAGGACGAAACACCGGT AATTTCTACTCTTGTAGAT).

Small scale flow cytometry experiments with VexGFP vectors

HT29 cells were transduced with virus for each of the guide+dCas12a-TAD-containing vectors separately; 5 d after transduction, cells were visualized by flow cytometry on a CytoFLEX S Sampler. To prepare samples for visualization, cells were stained with APC anti-human CD4 Antibody (Biolegend, 357408), diluted 1:100 for 20-30 minutes on ice.

Cells were washed with PBS two times to remove residual antibody and were resuspended in flow buffer (PBS, 2% FBS, 5 µM EDTA). CD4 signal was measured in the APC-A channel and VexGFP signal was measured in the K0525-A channel. Flow cytometry data were analyzed using FlowJo (v10.8.1). Cells were gated for VexGFP expression and APC gates were drawn such that ~1% of cells score as APC-positive in the control condition (stained parental cells).

Small scale flow cytometry experiments with nanobody vectors

HT29, MelJuSo, HCC2429, A549 and/or A375 cells were transduced with virus for each of the dCas12a-containing vectors separately; 2 d after transduction, cells were selected with blasticidin for 14 d. Blasticidin was removed for one passage and cells were subsequently transduced with virus for guide+nanobody-TAD-containing vectors. 2 d after transduction, cells were selected with puromycin for 5 d. Following selection, cells were visualized by flow cytometry on a CytoFLEX S Sampler at varying time points. To prepare samples for visualization, cells were stained with a fluorophore-conjugated antibody targeting the respective cell surface marker gene, diluted 1:100 for 20-30 minutes on ice.

CD4: APC anti-human CD4 antibody (Biolegend, 357408)
CD26 (DPP4): FITC anti-human CD26 antibody (Biolegend, 302704)
CD274: APC anti-human CD274 antibody (Biolegend, 329708)
CD97 (ADGRE5): FITC anti-human CD97 antibody (Biolegend, 336306)

Cells were washed with PBS two times to remove residual antibody and were resuspended in flow buffer (PBS, 2% FBS, 5 µM EDTA). Fluorophore signal was measured in the respective channel (APC-A or FITC-A). Flow cytometry data were analyzed using FlowJo (v10.8.1). Gates were set such that ~1% of cells score as APC-positive or FITC-positive in the control condition (stained parental cells).

RNA sequencing

Cells were cultivated as normal in preparation for RNA sequencing. When cells reached confluency, they were scraped from their flasks using cell scrapers, with existing media still present. 10 mL serological pipettes were used to break up cell clumps and cell-containing media was transferred to conicals. Cell mixtures were counted using a Coulter Counter to ensure that each pellet contained >1e6 cells. Cells were then pelleted by centrifugation at 321 x g for 5

minutes. Media was aspirated, pellets were resuspended in PBS, and the PBS-cell mixture was aliquoted into Eppendorf tubes. Cells were pelleted once more by centrifugation in a table-top centrifuge at maximum speed for 2 minutes. The supernatant was aspirated and pellets were flash frozen on dry ice, then frozen at -80 C, and submitted to Genewiz from Azenta Life Sciences for RNA extraction and sequencing.

QUANTIFICATION AND STATISTICAL ANALYSIS

Screen analysis

Guide sequences were extracted from sequencing reads by running the PoolQ tool with the search prefix “Position 1” (https://portals.broadinstitute.org/gpp/public/software/poolq). Reads were counted by alignment to a reference file of all possible guide RNAs present in the library. The read was then assigned to a condition (e.g. a well on the PCR plate) on the basis of the 8 nucleotide index included in the P7 primer. Following deconvolution, the resulting matrix of read counts was first normalized to reads per million within each condition by the following formula: read per guide RNA / total reads per condition x 1e6. Reads per million was then log2-transformed by first adding one to all values, which is necessary in order to take the log of guides with zero reads.

Prior to further analysis, we filtered out guides for which the log-normalized reads per million of the pDNA was > 3 standard deviations from the mean. We then calculated the log2-fold-change between conditions. All dropout (no drug) conditions were compared to the plasmid DNA (pDNA); drug-treated conditions were compared to the time-matched dropout sample. We assessed the correlation between log2-fold-change (LFC) values of replicates. LFC values were then z-scored based on the non-targeting guide controls. In the case of the genome-wide screens, guides targeting olfactory receptors were used in place of non-targeting controls for z-scoring.

RNA-seq analysis

RNA-seq was performed in triplicate for each experimental condition. Sequencing reads from Genewiz were aligned to the human Genome Reference Consortium Human Build 38 (hg38) using the STAR aligner. Transcript abundances were quantified using RNA-Seq by Expectation Maximization (RSEM). Differential expression was calculated using DESeq2 (v1.34.0) with shrunken LFC.

External datasets

CRISPRa Cas9 screens are from ref[33]

Data visualization

Figures were created with Python3, R studio, FlowJo 10.8.1, and GraphPad Prism (version 8). Schematics were created with BioRender.com.

Statistical analysis

All z-scores and correlation coefficients were calculated in Python.

DATA AVAILABILITY

Source data are provided with this paper. The read counts for all screening data, the mean fluorescence intensity values for all flow cytometry, and subsequent analyses are provided as Supplementary Data. Fastq files will be deposited in SRA and GEO.

CODE AVAILABILITY

All custom code used for analysis and example notebooks will be made available on GitHub: https://github.com/gpp-rnd/Cas12a-CRISPRa-Manuscript.

ACKNOWLEDGEMENTS

We thank all members of the Genetic Perturbation Platform; Desiree Hernandez, Berta Escude Velasco, Monica Roberson, Eliezer Josue Ibarra, Pema Tenzing, Tashi Lokyitsang, and Xiaoping Yang for producing guide libraries and lentivirus; Olivia Bare, Yenarae Lee, and Quinton Celuzza for logistics support; Matthew Greene, Bronte Wen, Doug Alan, Mark Tomko, and Tom Green for software engineering support; the Broad Institute Genomics Platform Walk-up Sequencing group for Illumina sequencing; the Functional Genomics Consortium for funding support; and Sarah Weiss, Ryan Steger, Priyanka Roy and Dany Gould for helpful discussions.

AUTHOR INFORMATION

Genetic Perturbation Platform, Broad Institute of MIT and Harvard, 75 Ames St, Cambridge, MA, USA
Audrey L Griffith, Fengyi Zheng, Abby V McGee, Nathan Miller, Ganna Reint, Yanjing V Liu, Amy Goodale & John G Doench

Zsofia Szegletes
Present address: University of California, Santa Barbara, CA, USA

Fabian Gademann
Present address: Utrecht University, Utrecht, Netherlands

Ifunanya Nwolah
Present address: Arbor Biotechnologies, Cambridge, MA, USA

Mudra Hegde
Present address: Thermo Fisher Scientific, Carlsbad, CA, USA

Contributions

Conceived of the study: JGD
Executed genetic screens: ALG, AVM, NM, GR, ZMS, FG, ISN, YVL
Performed analyses: ALG, FZ, ZMS
Created visualizations: ALG, AVM, AG, FZ
Designed libraries: JGD, FZ, MH
Curated data: ALG, FZ
Wrote the manuscript: ALG, AVM, AG, FZ, JGD
Supervised the project: JGD

ETHICS DECLARATIONS

JGD consults for Microsoft Research, Abata Therapeutics, Maze Therapeutics, BioNTech, Sangamo, and Pfizer. JGD consults for and has equity in Tango Therapeutics. JGD serves as a

762 paid scientific advisor to the Laboratory for Genomics Research, funded in part by GSK, and the
763 Innovative Genomics Institute, funded in part by Apple Tree Partners. JGD receives funding
764 support from the Functional Genomics Consortium: Abbvie, Bristol Myers Squibb, Janssen,
765 Merck, and Vir Biotechnology. JGD's interests are reviewed and managed by the Broad Institute
766 in accordance with its conflict of interest policies.

767 FIGURE LEGENDS

768 **Figure 1. Evaluation of existing Cas12a CRISPRa technologies. A**) Comparison of
769 CRISPRa constructs employing two different nuclease-deactivating mutations of Cas12a.
770 Activation was measured by the percentage of cells expressing CD4 five days after
771 transduction. **B**) CD4 mean fluorescence intensity (MFI) normalized to baseline expression
772 shown for 12 CRISPRa construct variants employing combinations of TADs directly tethered to
773 dCas12a (D908A). **C**) Schematic depicting overview of the flow cytometry-based tiling screen
774 performed to identify additional active Cas12a CRISPRa guides. **D**) Z-scores of the absolute
775 minimum LFC for each guide across technological replicates are plotted by the location of the
776 guide target site relative to the transcription start site (TSS) for CD4, CD26, CD97, and CD274.
777
778 **Figure 2. Nanobody recruitment improves CRISPRa activity. A**) Schematic representing
779 dCas12a nanobody-based recruitment of the transactivation domain (top). Plasmid maps
780 depicting one vector containing the ALFA tag fused to dCas12a and a second vector containing
781 the ALFA nanobody, TAD, and targeting guide (bottom). **B**) Heatmaps displaying comparative
782 performance between the p65, VP64, and Activ TADs when recruited via nanobody to dCas12a
783 harboring increasing numbers of ALFA tags (1x, 3x, 5x) at either the N- or C-terminus (N', C').
784 Experiments conducted in HT29, HCC2429, and A375 cell lines. Color scale reflects levels of
785 normalized MFI of CD4 expression within each cell line. **C**) Barplot illustrating combinatorial
786 effects emerging from the direct tethering of TADs to the N-terminus of dCas12a and nanobody-
787 based recruitment of varying TAD configurations to the N and/or C-termini. X-axis shows
788 normalized MFI values of CD4 expression on a log10 scale. **D**) Comparison of top-performers
789 from the direct tethering-based and nanobody-based TAD recruitment approaches. Histogram
790 shows the distribution of fluorescence peaks (left); barplots illustrate the percentage of cells
791 expressing CD4 (middle), and CD4 MFI values (right).
792
793 **Figure 3. Effective multiplexing with a nanobody-based system. A**) Schematic depicting
794 single-gene targeting guide cassette architecture (top). Histograms show expression levels of
795 CD4 (APC), CD274 (APC), CD97 (FITC), and CD26 (FITC) in HT29, A375, and HCC2429 cells
796 expressing 5x-tag-dCas12a-VP64 when targeted individually by three guides per gene paired
797 with nanobody-VP64, nanobody-p65, or nanobody-p65-HSF1 (bottom). Data from one
798 representative replicate shown; data for all replicates is included in Supplementary Data 2. **B**)
799 Schematic depicting multiplexed targeting guide cassette architecture (top). Heatmaps of
800 normalized MFI values for CD26, CD4, CD97, and CD274 in HT29, A375, and HCC2429 cells
801 expressing 5x-tag-dCas12a-VP64 when targeted simultaneously by one guide per gene paired
802 with nanobody-VP64, nanobody-p65, or nanobody-p65-HSF1. MFI values were normalized to
803 basal expression within each cell line/gene combination, as is the color scale (bottom). **C**)
804 Comparison of RNA expression levels across samples expressing 5x-tag-dCas12a-VP64 and

either nanobody-VP64 or nanobody-p65 with or without three CD4-targeting guides. Shrunken LFC in the CD4-targeting population is plotted against mean normalized read counts of all replicates for baseline expression (n = 3).

Figure 4. Development of Cas12a genome-wide activation libraries. A) Schematic representing dCas12a screening approach encompassing the “wide” [-450 to 375] and “narrow” [-300 to 0] targeting windows relative to the annotated TSS; each gene is targeted by 6 guides (3 in Set A and 3 in Set B). Both sets for the two targeting windows were tested with the p65 and VP64 nanobody approach. **B**) Scatter plot comparing the p65 and VP64 nanobody approaches in the viability arm (left) and selumetinib drug arm (right), with select genes highlighted. **C**) Venn diagrams showing overlapping top 100 genes between the dCas9, dCas12a, and ORF selumetinib modifier screens for resistance and sensitization.

Figure 5. Validation of primary screen hits to learn on-rules for effective targeting. A) Scatterplot of z-scores comparing all triple-guide constructs in both primary and secondary screens. Each triple-guide construct has z-scores calculated in four screen arms: VP64 viability, VP64 selumetinib, p65 viability, p65 selumetinib (n = 8416 constructs). **B**) Comparison of z-score distributions for single, dual, or triple-guide constructs targeting highest confidence genes in the selumetnib arm: sensitizing genes (constructs = 291, left) and resistant genes (constructs = 346, right). Boxes show the quartiles (Q1 and Q3) as minima and maxima and the center represents the median; whiskers show 1.5 times the interquartile range (Q1 - 1.5*IQR and Q3 + 1.5*IQR). **C**) Scatterplots of z-score between dual-guide and single-guides targeting highest confidence selumetinib sensitizing genes (number of dual guides = 240, left), selumetinib resistant genes (number of dual guides = 286, middle), and growth-inhibitory genes (number of dual guides = 382, right). Pearson correlations of z-scores between dual-guides and best performing single guides and worst performing single guides are highlighted in the upper left and lower right corners, respectively. **D**) enPAM+GB scores for single-guide constructs, binned by z-score. There are 109 guides in the low active bin (|z-score| <= 1), 42 guides in the median active bin (1 < |z-score| <= 2), and 51 guides in the highly active bin (|z-score| > 2). **E**) Fraction of guides in each activity bin for single-guide constructs targeting the high confidence gene set relative to MANE select TSS. **F**) Fraction of guides in each activity bin for single-guide constructs targeting the high confidence gene set relative to MANE select TSS and enPAM+GB.

SUPPLEMENTARY FIGURES

Supplementary Figure 1. Identification of active Cas12a CRISPRa guides. A) Log-fold change of all guides in the first position when paired with ten different CD4-targeting guides in the second position. LFC is calculated by subtracting the maximum log-normalized read count score across the replicates of the CD4-negative sorted population from the minimum score across the replicates of the CD4-positive sorted population. Boxes show the quartiles (Q1 and Q3) as minima and maxima and the center represents the mean; whiskers show 1.5 times the interquartile range (Q1 - 1.5*IQR and Q3 + 1.5*IQR). **B**) Gating strategy used to assess fluorescence in the APC (CD4) and KO525 (VexGFP) channels. Stained parental HT29 cells were gated first for live cells. This live cell population was then gated to exclude doublets, and

849 the single cell population was further gated to exclude cells with below baseline levels of KO525
850 fluorescence. All three gates were extrapolated to all samples and the respective KO525-
851 positive (VexGFP+) populations were used to assess fluorescence intensity in the APC channel.
852 **C**) LFC correlations for all technological replicates of the flow-sorted samples from the tiling
853 library. Plots are shown for HT29 and A375 cells expressing dCas12a-VP64 or VP64-dCas12a-
854 VP64, sorted for expression of CD97, CD26, CD274, or CD4. LFCs were calculated by
855 subtracting sorted samples from one another (positive - negative sorted population).
856
857 **Supplementary Figure 2. Optimization of nanobody recruitment for CRISPRa. A**)
858 Comparison of CRISPRa activity when a nanobody-TAD combination is recruited to the N' or C'
859 terminus of Cas12a tethered to VP64 (N' 5x-tag, C' 5x-tag). Each dot represents one nanobody-
860 TAD combination recruited to either the N' or C' terminus of dCas12a-VP64. Normalized CD4
861 MFI values are shown for three cell lines (A375, HT29, and HCC2429). Dotted line depicts the
862 line of identity (x = y). **B**) Comparison of CRISPRa activity in HT29 cells expressing VP64-
863 dCas12a-3x-tag when either p65, p65-HSF1, VP64 and p65-HSF1, or p65 and p65-HSF1 are
864 recruited via nanobody. Histogram shows the distribution of fluorescence peaks (left) and
865 barplot shows normalized CD4 MFI values (right). Stained parental cells are depicted in gray. **C**)
866 Assessment of the effect of an additional NLS on the C-terminus of the nanobody-p65 construct
867 on CD4 activation efficiency in HT29 cells. Histogram shows the distribution of fluorescence
868 peaks (left) and barplot shows normalized CD4 MFI values (right). Stained parental cells are
869 depicted in gray.
870
871 **Supplementary Figure 3. Examination of nanobody-based Cas12a CRISPRa specificity**
872 **via RNA-seq analysis. A**) Summary table of five samples being compared in subsequent
873 analyses for differential gene expression, as assessed by bulk RNA sequencing of HT29 cells.
874 **B**) Comparison of RNA expression levels across samples expressing 5x-tag-dCas12a-VP64
875 and nanobody or nanobody-p65 (left) and nanobody or nanobody-VP64 (middle) without CD4-
876 targeting guides. Shrunken LFC in the TAD-expressing population (nanobody-VP64 or
877 nanobody-p65) is plotted against mean normalized read counts of all replicates for baseline
878 expression (n = 3). **C**) Comparison of RNA expression levels across samples expressing 5x-tag-
879 dCas12a-VP64 and nanobody-VP64 with or without CD4-targeting guides (left) or nanobody-
880 p65 with or without CD4-targeting guides (right). Shrunken LFC is plotted for genes within 500
881 kb upstream or downstream of the transcription start site of CD4 (n = 40 genes).
882
883 **Supplementary Figure 4. Development of Cas12a genome-wide activation libraries. A**) Z-
884 scored LFC for guides targeting seven members of the cyclin-dependent kinase inhibitor family.
885 Each dot represents the construct-level z-score, showing both the p65 and VP64 TAD results.
886 Boxes show the quartiles (Q1 and Q3) as minima and maxima and the center represents the
887 median; whiskers show 1.5 times the interquartile range (Q1 - 1.5*IQR and Q3 + 1.5*IQR). **B**)
888 Replicate correlations (Pearson's r) for viability and selumetinib modifier ORF screens. **C**) Venn
889 diagrams showing overlapping top 100 genes between the dCas9, dCas12a, and ORF viability
890 screens, ranked by z-score for growth-promoting (left) and growth-inhibitory (right) directions.
891

892 **Supplementary Figure 5. Validation libraries. A**) Table with numbers of hit genes that scored
893 with |z-score| >2 with VP64 or p65 in the viability and selumetinib primary screens that were
894 then included in the validation library (left). Schematic depicting validation library assembly
895 (right). **B**) Replicate correlations (Pearson's r) for both validation libraries screened with 5x-tag-
896 dCas12a-VP64 cells in duplicate for the viability arm (top) and selumetinib arm (bottom). **C**)
897 Comparison of z-score distributions for single, dual, or triple-guide constructs targeting highest
898 confidence growth-inhibitory genes (constructs = 475) in secondary screens. Boxes show the
899 quartiles (Q1 and Q3) as minima and maxima and the center represents the median; whiskers
900 show 1.5 times the interquartile range (Q1 - 1.5*IQR and Q3 + 1.5*IQR). **D**) Heatmaps of
901 Pearson's correlation for z-scores of all six three-guide construct permutations in the viability
902 arm (top) and selumetinib arm (bottom) for the 142 overlapping hits between VP64 and p65 in
903 the primary screen (n = 3407 constructs).
904
905 SUPPLEMENTARY DATA
906 **Title:** Supplementary Data 1.
907 **Description:** Cas12a flow tiling screens - read counts, library annotation, replicate correlations.
908 Associated with Fig 1.
909
910 **Title:** Supplementary Data 2.
911 **Description:** Flow cytometry data - raw MFI values, MFI values normalized to baseline parental
912 expression, percent positive metrics for each sample. Associated with Figs 1,2,3.
913
914 **Title:** Supplementary Data 3.
915 **Description:** Genome-wide Cas12a CRISPRa screens - read counts, library annotation,
916 replicate correlations. Associated with Fig 4.
917
918 **Title:** Supplementary Data 4.
919 **Description:** ORF screens - read counts, library annotation, replicate correlations. Associated
920 with Fig 4.
921
922 **Title:** Supplementary Data 5.
923 **Description:** Secondary Cas12a CRISPRa screens - read counts, library annotation, replicate
924 correlations. Associated with Fig 5.
925
926
927
928
929 REFERENCES

930 1. Qi, L. S. *et al.* Repurposing CRISPR as an RNA-guided platform for sequence-specific control of
931 gene expression. *Cell* **152**, 1173–1183 (2013).
932 2. Gilbert, L. A. *et al.* CRISPR-mediated modular RNA-guided regulation of transcription in eukaryotes.
933 *Cell* **154**, 442–451 (2013).
934 3. Beerli, R. R., Dreier, B. & Barbas, C. F., 3rd. Positive and negative regulation of endogenous genes
935 by designed transcription factors. *Proc. Natl. Acad. Sci. U. S. A.* **97**, 1495–1500 (2000).
936 4. Perez-Pinera, P. *et al.* Synergistic and tunable human gene activation by combinations of synthetic

937 transcription factors. *Nat. Methods* **10**, 239–242 (2013).
938 5. Maeder, M. L. *et al.* Robust, synergistic regulation of human gene expression using TALE activators.
939 *Nat. Methods* **10**, 243–245 (2013).
940 6. Hilton, I. B. *et al.* Epigenome editing by a CRISPR-Cas9-based acetyltransferase activates genes
941 from promoters and enhancers. *Nat. Biotechnol.* **33**, 510–517 (2015).
942 7. Maeder, M. L., Cascio, V. M., Fu, Y., Ho, Q. H. & Joung, J. K. CRISPR RNA–guided activation of
943 endogenous human genes. *Nat. Methods* **10**, 977–979 (2013).
944 8. Konermann, S. *et al.* Genome-scale transcriptional activation by an engineered CRISPR-Cas9
945 complex. *Nature* **517**, 583–588 (2015).
946 9. Tanenbaum, M. E., Gilbert, L. A., Qi, L. S., Weissman, J. S. & Vale, R. D. A protein-tagging system
947 for signal amplification in gene expression and fluorescence imaging. *Cell* **159**, 635–646 (2014).
948 10. Chavez, A. *et al.* Highly efficient Cas9-mediated transcriptional programming. *Nat. Methods* **12**, 326–
949 328 (2015).
950 11. Tycko, J. *et al.* High-Throughput Discovery and Characterization of Human Transcriptional Effectors.
951 *Cell* **183**, 2020–2035.e16 (2020).
952 12. Alerasool, N., Leng, H., Lin, Z.-Y., Gingras, A.-C. & Taipale, M. Identification and functional
953 characterization of transcriptional activators in human cells. *Mol. Cell* **82**, 677–695.e7 (2022).
954 13. DelRosso, N. *et al.* Large-scale mapping and mutagenesis of human transcriptional effector domains.
955 *Nature* (2023) doi:10.1038/s41586-023-05906-y.
956 14. Leng, K. *et al.* CRISPRi screens in human iPSC-derived astrocytes elucidate regulators of distinct
957 inflammatory reactive states. *Nat. Neurosci.* (2022) doi:10.1038/s41593-022-01180-9.
958 15. Rebendenne, A. *et al.* Bidirectional genome-wide CRISPR screens reveal host factors regulating
959 SARS-CoV-2, MERS-CoV and seasonal HCoVs. *Nat. Genet.* **54**, 1090–1102 (2022).
960 16. Tak, Y. E. *et al.* Augmenting and directing long-range CRISPR-mediated activation in human cells.
961 *Nat. Methods* **18**, 1075–1081 (2021).
962 17. Bell, C. C. *et al.* Transcription factors use a unique combination of cofactors to potentiate different
963 promoter-dependent steps in transcription. *bioRxiv* 2022.10.25.513774 (2022)
964 doi:10.1101/2022.10.25.513774.
965 18. Radzisheuskaya, A., Shlyueva, D., Müller, I. & Helin, K. Optimizing sgRNA position markedly
966 improves the efficiency of CRISPR/dCas9-mediated transcriptional repression. *Nucleic Acids Res.*
967 **44**, e141 (2016).
968 19. DeWeirdt, P. C. *et al.* Optimization of AsCas12a for combinatorial genetic screens in human cells.
969 *Nat. Biotechnol.* **39**, 94–104 (2021).
970 20. Kleinstiver, B. P. *et al.* Engineered CRISPR-Cas12a variants with increased activities and improved
971 targeting ranges for gene, epigenetic and base editing. *Nat. Biotechnol.* (2019) doi:10.1038/s41587-
972 018-0011-0.
973 21. Sack, L. M., Davoli, T., Xu, Q., Li, M. Z. & Elledge, S. J. Sources of Error in Mammalian Genetic
974 Screens. *G3* **6**, 2781–2790 (2016).
975 22. Hegde, M., Strand, C., Hanna, R. E. & Doench, J. G. Uncoupling of sgRNAs from their associated
976 barcodes during PCR amplification of combinatorial CRISPR screens. *PLoS One* **13**, e0197547
977 (2018).
978 23. Replogle, J. M. *et al.* Maximizing CRISPRi efficacy and accessibility with dual-sgRNA libraries and
979 optimal effectors. *bioRxiv* 2022.07.13.499814 (2022) doi:10.1101/2022.07.13.499814.
980 24. Gier, R. A. *et al.* High-performance CRISPR-Cas12a genome editing for combinatorial genetic
981 screening. *Nat. Commun.* **11**, 3455 (2020).
982 25. Dede, M., McLaughlin, M., Kim, E. & Hart, T. Multiplex enCas12a screens detect functional buffering
983 among paralogs otherwise masked in monogenic Cas9 knockout screens. *Genome Biol.* **21**, 262
984 (2020).
985 26. Li, R. *et al.* Comparative optimization of combinatorial CRISPR screens. *Nat. Commun.* **13**, 1–10
986 (2022).
987 27. Campa, C. C., Weisbach, N. R., Santinha, A. J., Incarnato, D. & Platt, R. J. Multiplexed genome
988 engineering by Cas12a and CRISPR arrays encoded on single transcripts. *Nat. Methods* (2019)
989 doi:10.1038/s41592-019-0508-6.
990 28. Vora, S. *et al.* Rational design of a compact CRISPR-Cas9 activator for AAV-mediated delivery.
991 *bioRxiv* 298620 (2018) doi:10.1101/298620.
992 29. Doench, J. G. Am I ready for CRISPR? A user's guide to genetic screens. *Nat. Rev. Genet.* **19**, 67–

80 (2018).
30. Götzke, H. *et al.* The ALFA-tag is a highly versatile tool for nanobody-based bioscience applications. *Nat. Commun.* **10**, 4403 (2019).
31. Love, M. I., Huber, W. & Anders, S. Moderated estimation of fold change and dispersion for RNA-seq data with DESeq2. *Genome Biol.* **15**, 550 (2014).
32. Zhu, A., Ibrahim, J. G. & Love, M. I. Heavy-tailed prior distributions for sequence count data: removing the noise and preserving large differences. *Bioinformatics* **35**, 2084–2092 (2019).
33. Sanson, K. R. *et al.* Optimized libraries for CRISPR-Cas9 genetic screens with multiple modalities. *Nat. Commun.* **9**, 5416 (2018).
34. van der Meer, D. *et al.* Cell Model Passports-a hub for clinical, genetic and functional datasets of preclinical cancer models. *Nucleic Acids Res.* **47**, D923–D929 (2019).
35. Knackmuss, U. *et al.* MAP3K11 is a tumor suppressor targeted by the oncomiR miR-125b in early B cells. *Cell Death Differ.* **23**, 242–252 (2016).
36. Sack, L. M. *et al.* Profound Tissue Specificity in Proliferation Control Underlies Cancer Drivers and Aneuploidy Patterns. *Cell* **173**, 499–514.e23 (2018).
37. Ito, T. *et al.* Paralog knockout profiling identifies DUSP4 and DUSP6 as a digenic dependence in MAPK pathway-driven cancers. *Nat. Genet.* **53**, 1664–1672 (2021).
38. Meng, Y. *et al.* GATA6 phosphorylation by Erk1/2 propels exit from pluripotency and commitment to primitive endoderm. *Dev. Biol.* **436**, 55–65 (2018).
39. Hart, T. *et al.* High-Resolution CRISPR Screens Reveal Fitness Genes and Genotype-Specific Cancer Liabilities. *Cell* **163**, 1515–1526 (2015).
40. Yang, X. *et al.* A public genome-scale lentiviral expression library of human ORFs. *Nat. Methods* **8**, 659–661 (2011).
41. Rees, M. G. *et al.* Systematic identification of biomarker-driven drug combinations to overcome resistance. *Nat. Chem. Biol.* **18**, 615–624 (2022).
42. Horlbeck, M. A. *et al.* Compact and highly active next-generation libraries for CRISPR-mediated gene repression and activation. *Elife* **5**, (2016).
43. Amabile, A. *et al.* Inheritable Silencing of Endogenous Genes by Hit-and-Run Targeted Epigenetic Editing. *Cell* **167**, 219–232.e14 (2016).
44. Holtzman, L. & Gersbach, C. A. Editing the Epigenome: Reshaping the Genomic Landscape. *Annu. Rev. Genomics Hum. Genet.* **19**, 43–71 (2018).
45. Nuñez, J. K. *et al.* Genome-wide programmable transcriptional memory by CRISPR-based epigenome editing. *Cell* (2021) doi:10.1016/j.cell.2021.03.025.
46. Chardon, F. M. *et al.* Multiplex, single-cell CRISPRa screening for cell type specific regulatory elements. *bioRxiv* (2023) doi:10.1101/2023.03.28.534017.

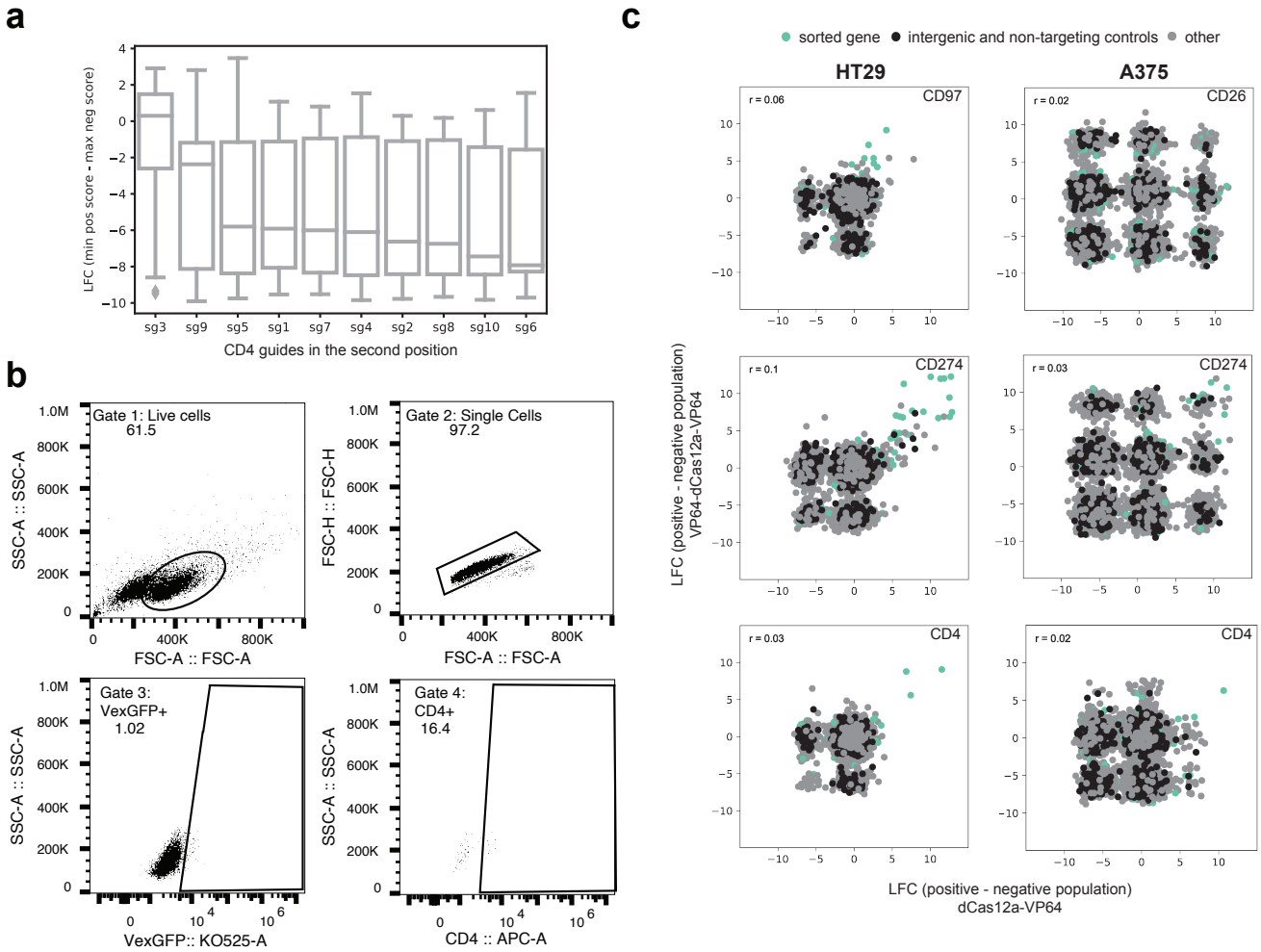

Supplementary Figure 1. Identification of active Cas12a CRISPRa guides. A) Log-fold change of all guides in the first position when paired with ten different CD4-targeting guides in the second position. LFC is calculated by subtracting the maximum log-normalized read count score across the replicates of the CD4-negative sorted population from the minimum score across the replicates of the CD4-positive sorted population. Boxes show the quartiles (Q1 and Q3) as minima and maxima and the center represents the mean; whiskers show 1.5 times the interquartile range (Q1 - 1.5*IQR and Q3 + 1.5*IQR). B) Gating strategy used to assess fluorescence in the APC (CD4) and KO525 (VexGFP) channels. Stained parental HT29 cells were gated first for live cells. This live cell population was then gated to exclude doublets, and the single cell population was further gated to exclude cells with below baseline levels of KO525 fluorescence. All three gates were extrapolated to all samples and the respective KO525-positive (VexGFP+) populations were used to assess fluorescence intensity in the APC channel. C) LFC correlations for all technological replicates of the flow-sorted samples from the tiling library. Plots are shown for HT29 and A375 cells expressing dCas12a-VP64 or VP64-dCas12a-VP64, sorted for expression of CD97, CD26, CD274, or CD4. LFCs were calculated by subtracting sorted samples from one another (positive - negative sorted population).

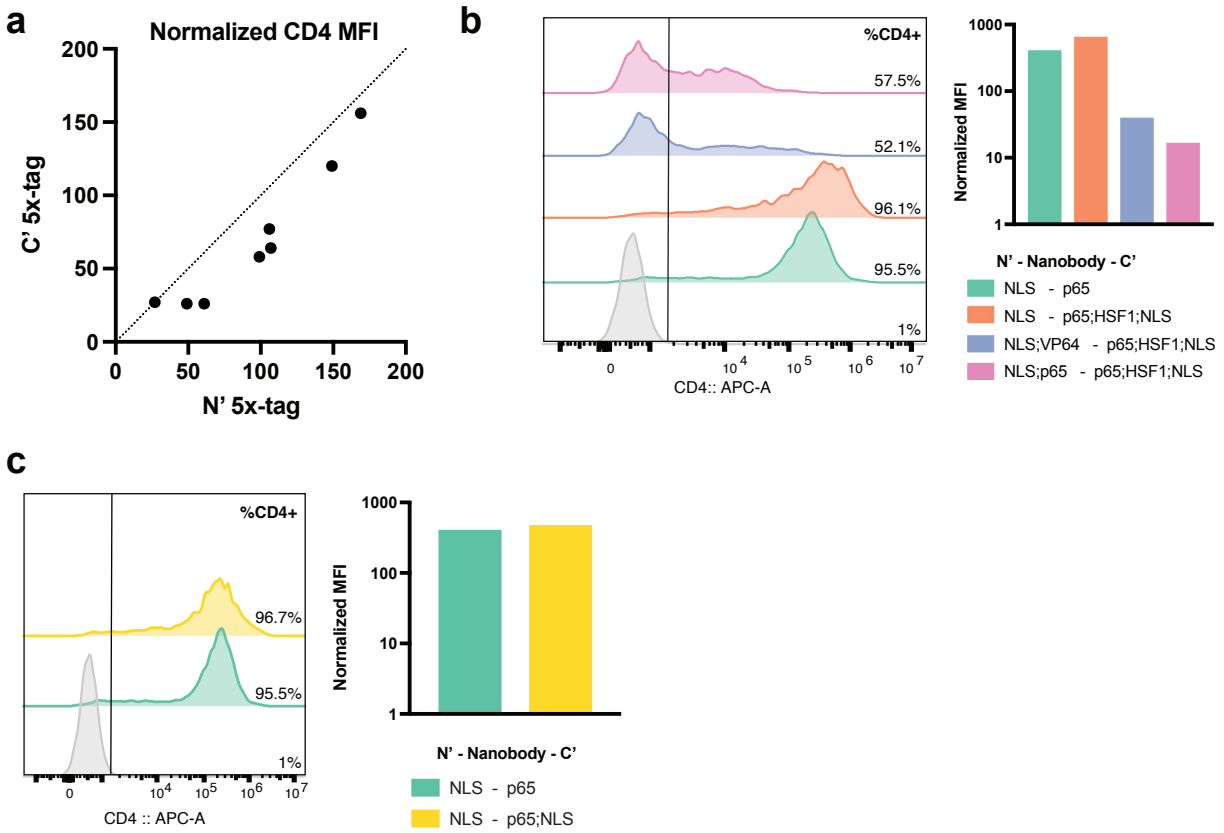

Supplementary Figure 2. Optimization of nanobody recruitment for CRISPRa. A) Comparison of CRISPRa activity when a nanobody-TAD combination is recruited to the N' or C' terminus of Cas12a tethered to VP64 (N' 5x-tag, C' 5x-tag). Each dot represents one nanobody-TAD combination recruited to either the N' or C' terminus of dCas12a-VP64. Normalized CD4 MFI values are shown for three cell lines (A375, HT29, and HCC2429). Dotted line depicts the line of identity (x = y). B) Comparison of CRISPRa activity in HT29 cells expressing VP64-dCas12a-3x-tag when either p65, p65-HSF1, VP64 and p65-HSF1, or p65 and p65-HSF1 are recruited via nanobody. Histogram shows the distribution of fluorescence peaks (left) and barplot shows normalized CD4 MFI values (right). Stained parental cells are depicted in gray. C) Assessment of the effect of an additional NLS on the C-terminus of the nanobody-p65 construct on CD4 activation efficiency in HT29 cells. Histogram shows the distribution of fluorescence peaks (left) and barplot shows normalized CD4 MFI values (right). Stained parental cells are depicted in gray.

a

dCas12a	Nanobody	CD4-Targeting Guide	Sample Name
5x-tag-dCas12a	nanobody	No	A
5x-tag-dCas12a-VP64	nanobody-p65	Yes	B
		No	C
	nanobody-VP64	Yes	D
		No	E

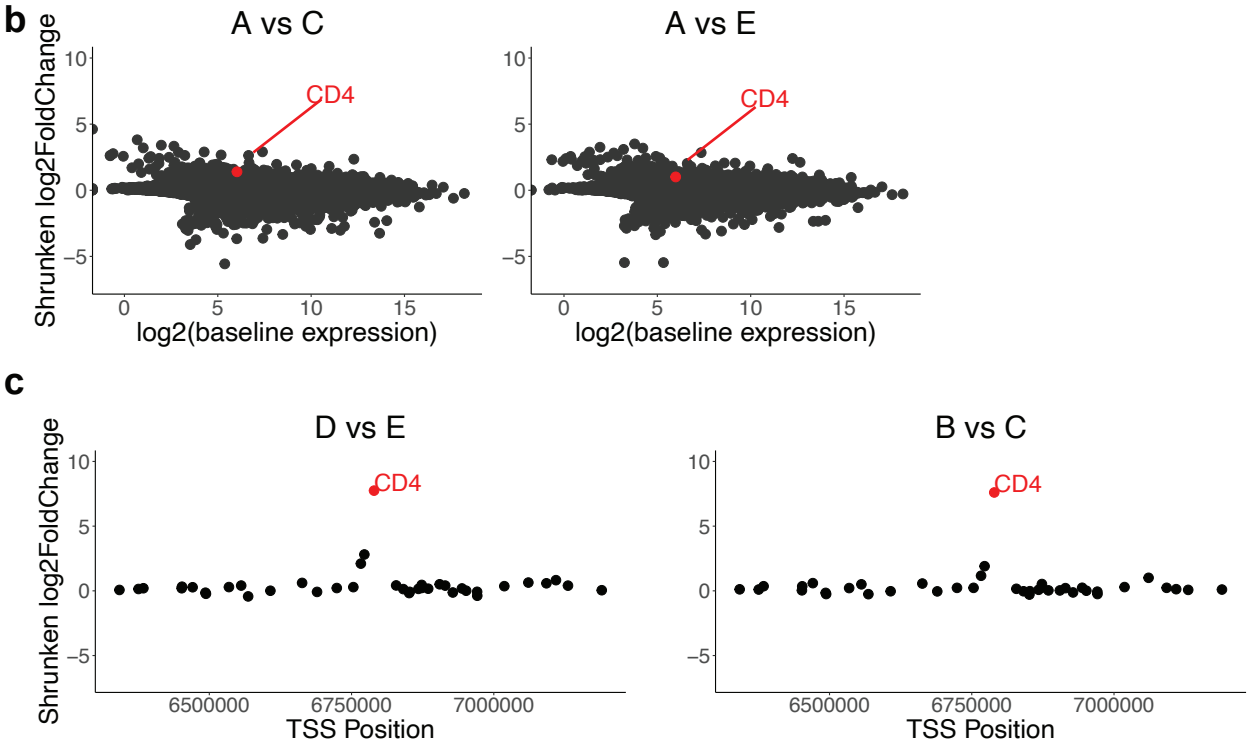

Supplementary Figure 3. Examination of nanobody-based Cas12a CRISPRa specificity via RNA-seq analysis. A) Summary table of five samples being compared in subsequent analyses for differential gene expression, as assessed by bulk RNA sequencing of HT29 cells. B) Comparison of RNA expression levels across samples expressing 5x-tag-dCas12a-VP64 and nanobody or nanobody-p65 (left) and nanobody or nanobody-VP64 (middle) without CD4-targeting guides. Shrunken LFC in the TAD-expressing population (nanobody-VP64 or nanobody-p65) is plotted against mean normalized read counts of all replicates for baseline expression (n = 3). C) Comparison of RNA expression levels across samples expressing 5x-tag-dCas12a-VP64 and nanobody-VP64 with or without CD4-targeting guides (left) or nanobody-p65 with or without CD4-targeting guides (right). Shrunken LFC is plotted for genes within 500 kb upstream or downstream of the transcription start site of CD4 (n = 40 genes).

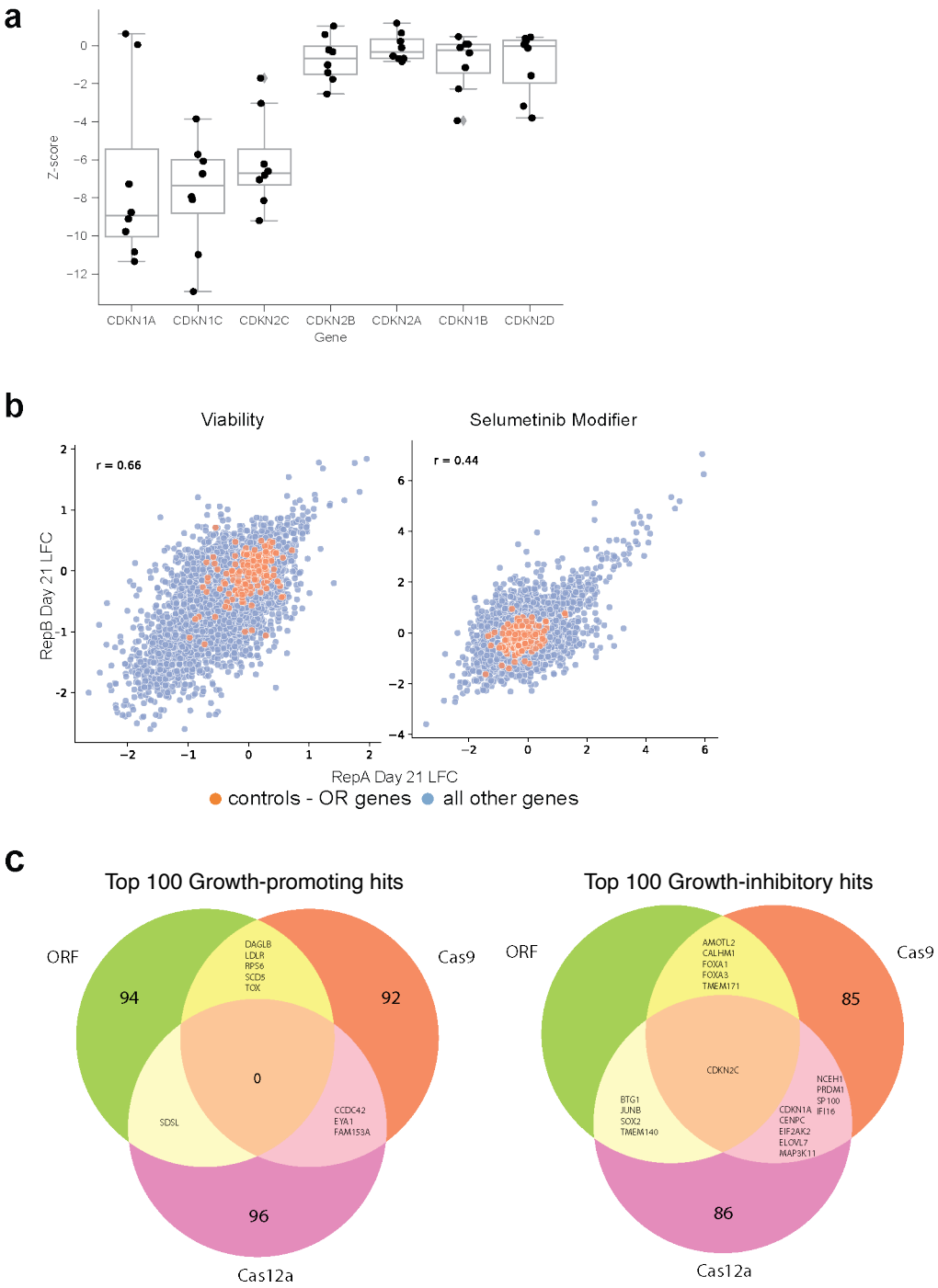

Supplementary Figure 4. Development of Cas12a genome-wide activation libraries. A) Z-scored LFC for guides targeting seven members of the cyclin-dependent kinase inhibitor family. Each dot represents the construct-level z-score, showing both the p65 and VP64 TAD results. Boxes show the quartiles (Q1 and Q3) as minima and maxima and the center represents the median; whiskers show 1.5 times the interquartile range (Q1 - 1.5*IQR and Q3 + 1.5*IQR). B) Replicate correlations (Pearson's r) for viability and selumetinib modifier ORF screens. C) Venn diagrams showing overlapping top 100 genes between the dCas9, dCas12a, and ORF viability screens, ranked by z-score for growth-promoting (left) and growth-inhibitory (right) directions.

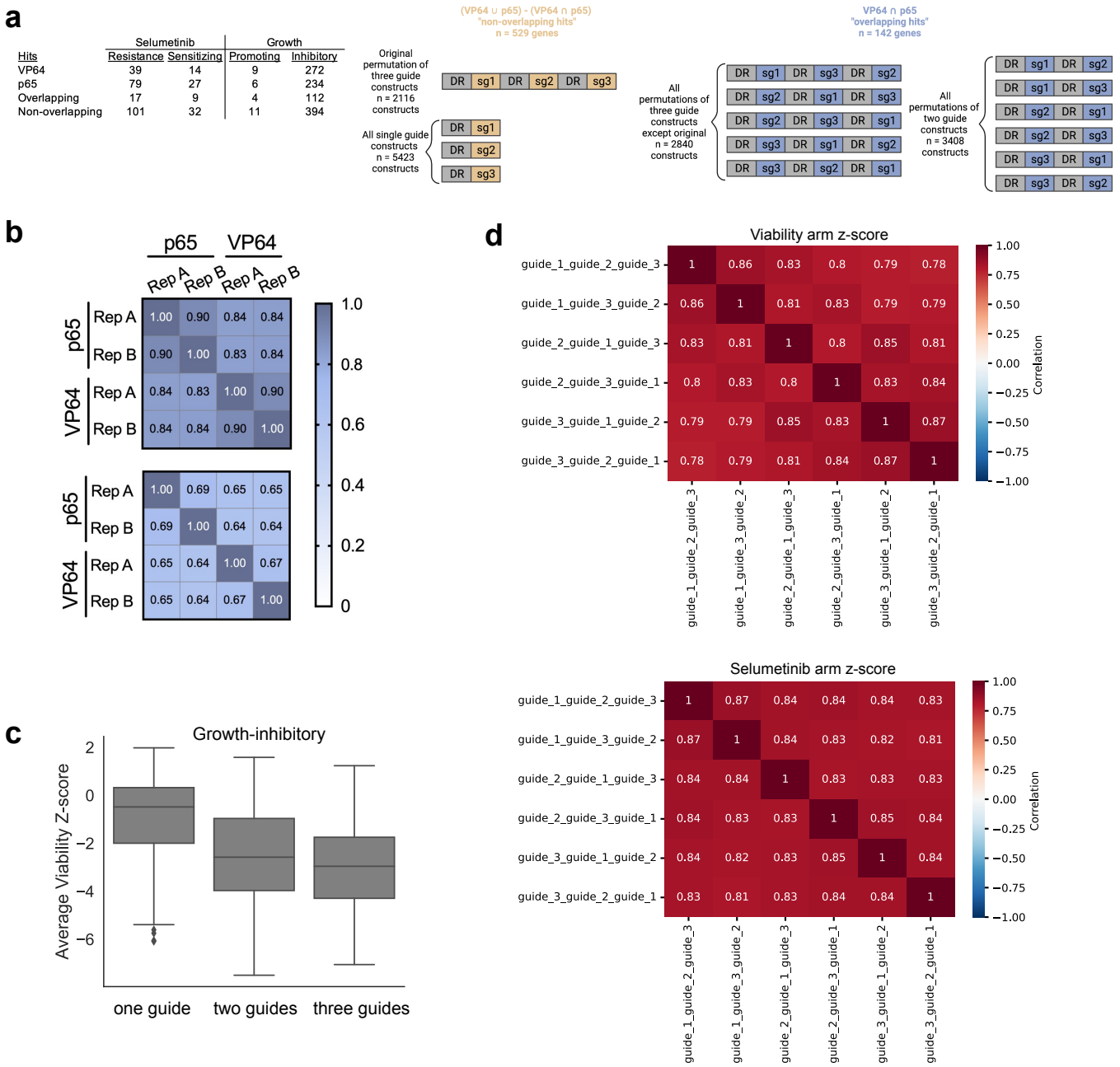

Supplementary Figure 5. Validation libraries. A) Table with numbers of hit genes that scored with |z-score| >2 with VP64 or p65 in the viability and selumetinib primary screens that were then included in the validation library (left). Schematic depicting validation library assembly (right). B) Replicate correlations (Pearson's r) for both validation libraries screened with 5x-tag-dCas12a-VP64 cells in duplicate for the viability arm (top) and selumetinib arm (bottom). C) Comparison of z-score distributions for single, dual, or triple-guide constructs targeting highest confidence growth-inhibitory genes (constructs = 475) in secondary screens. Boxes show the quartiles (Q1 and Q3) as minima and maxima and the center represents the median; whiskers show 1.5 times the interquartile range (Q1 - 1.5*IQR and Q3 + 1.5*IQR). D) Heatmaps of Pearson's correlation for z-scores of all six three-guide construct permutations in the viability arm (top) and selumetinib arm (bottom) for the 142 overlapping hits between VP64 and p65 in the primary screen (n = 3407 constructs).